Energy, Mines and Resources Canada
Énergie, Mines et Ressources Canada

CANMET
Canada Centre for Mineral and Energy Technology
Centre canadien de la technologie des minéraux et de l'énergie

HIGH STRENGTH CAST NICKEL-ALUMINUM BRONZES

M. SAHOO
METALLURGY SECTION

JUNE, 1982

This document was produced for internal distribution and internal reporting purposes. It does not represent a final expression of the opinion of the Canada Centre for Mineral and Energy Technology (CANMET)

Ce document a été produit pour fins de diffusion et de documentation internes. Il ne représente aucunement l'expression définitive de l'opinion du Centre canadien de la technologie des minéraux et de l'énergie (CANMET)

MINERALS RESEARCH PROGRAM

PHYSICAL METALLURGY RESEARCH LABORATORIES

REPORT: MRP/PMRL 82-44(TR)

PHYSICAL METALLURGY RESEARCH LABORATORIES
REPORT MRP/PMRL 82-44(TR)

HIGH STRENGTH CAST NICKEL-ALUMINUM BRONZES

by

M. Sahoo

ABSTRACT

The microstructure and mechanical properties of continuously cast, simulated - sand cast, sand-cast, and welded - sand-cast nickel-aluminum bronze (NAB) alloys have been evaluated over a range of aluminum contents and Ni:Fe ratios. The influence of the corrosion-inhibiting heat treatment of 6 h at 700°C on the structure and properties has also been examined.

It is shown that, because of changes in the precipitates within the α phase, the corrosion-inhibiting heat treatment causes an increase in tensile and yield strength, and a reduction in elongation and CVN impact properties, as well as reducing or eliminating γ_2 from the microstructures.

It is also shown that when Ni-Al bronze filler wire is used, deleterious γ_2 phase is formed in both the fusion and heat affected zones. Post-weld heat treatment is effective in eliminating γ_2 from such regions. Heat treatment causes spheroidization of κ constituents in the fusion and heat affected zones, induces fine precipitates in the α phase of the base metal and, thus, increases strength and reduces ductility. Although impact properties were reduced by the corrosion-inhibiting heat treatment, an impact value of 27 J (20 ft-lb) was obtained at room temperature irrespective of the filler wire and base metal composition.

The new "low aluminum" filler wire produces welds of improved quality with inherently good corrosion resistance. Use of the wire to weld or repair castings followed by post-weld heat treatment of the casting is commercially practicable and technically advantageous.

INTRODUCTION

Ni-Al bronze (NAB) alloys conforming to ASTM B148 alloy C95800 are used extensively for marine castings because of their high strength, moderate ductility and reasonable corrosion resistance, when used in the correct microstructural condition. These alloys are, however, subject to selective phase attack (dealuminification), especially in the heat-affected zone (HAZ) of welds when no post-weld heat treatment is applied. Dealuminification occurs because of the presence of γ_2 phase.

Previous studies of the nickel-aluminum bronze alloys have shown the effect of composition on properties (1,2) and have demonstrated the effect of iron and nickel content on the formation, composition and morphology of the iron-rich (Fe_3Al) and nickel-rich (NiAl) κ phase (3). In the present work, the mechanical properties and microstructure of alloys at the low aluminum (~8.5% Al) end of the composition range were investigated. Particular study was made of the occurence of the two-phase $\alpha + \gamma_2$ structure (which is known to induce corrosion) and its removal by a corrosion-inhibiting heat treatment (6-8 h at 650-700°C followed by air cooling) which has been reported most recently by Zanis and Ferrara (4,5).

Because weld-repairing of NAB alloy castings is done quite frequently, the present work also studied the weldability of sand-cast alloys and examined the effect of the corrosion-inhibiting heat treatment on the structure and mechanical properties of constrained butt-welded alloys over a range of aluminum contents and Ni:Fe ratios.

Because of the susceptibility of complex NAB alloys to cracking, procedures call for MIG process weld repairs to be made with two different filler wires (6). Thus, a Cu-Al-Fe alloy (Ampcotrode 10) containing ~10% aluminum is used first to fill the bulk of the excavated area. The inherent ductility of this nickel-free alloy allows crack-free welds to be obtained. However, because this alloy is prone to selective corrosive attack of the β-phase in sea water, the final two passes are made with the corrosion-resistant Ni-Al bronze filler wire (Ampcotrode 46). The structure and mechanical properties of welds made by this "buttering" technique have also been determined.

Research to date indicates that "low aluminum" (8.5% Al) NAB alloy should be used in commercial practice (8) throughout the weld, or just for buttering. However, commercial filler wires for welding these alloys usually

contain 9-9.5% Al, although the code specifies 8.5-9.5% Al. In this work, an attempt has been made to develop a low-aluminum filler wire matching the strength and composition of the parent metal, and to compare the structure and mechanical properties of the weldments made with this wire with weldments made with Ampcotrode 46 filler wire (9.4% Al).

The significant results of this project are summarized in this final report. A complete description of the experimental work and the results obtained can be found in previous reports (7-17).

2. EXPERIMENTAL PROCEDURE

2.1 MELTING AND CASTING

Continuously cast rods, 22 mm (7/8 in.) in diam were produced to prepare the large number of alloys withing the selected composition range shown in Table 1. The laboratory-built vertical continuous casting machine was operated at a production rate of 305 mm (12 in.) min^{-1}, using intermittent extraction parameters of t_{ON}=0.25 s (go period), t_{OFF}=1.5 s (stop period) at a nominal peripheral extraction roll speed of 3 m (120 in.) min^{-1}. The water-jacketed graphite mould, reamed to 22 mm (0.875 in.) diam. and 152 mm (6 in.) in length, was cemented to a 20 kg (45 lb) capacity induction heated clay-graphite crucible. Pre-alloyed melt stock was melted in-situ in the casting machine holding furnace, and fused to an aluminum bronze starter bar inserted into the mould. The tundish metal temperature during casting was maintained at 1200°C under a nitrogen blanket. Measured quantities (4.5 m, 15 ft) of bar were cast at each of three aluminum levels per heat. The compositions of the experimental alloys are given in Table 2.

Simulated sand cast structures were produced in this continuously cast rod by homogenizing for 2 h at 1000°C, followed by furnace cooling at about 4°C per min to 500°C , and then air cooling to room temperature.

Companion melts (cast into modified keel blocks) were made of selected compositions using standard 60 kg (130 lb) induction air-melting techniques (Table 3).

Tensile specimens of 13 mm (0.505 in.) diameter by 51 mm (2 in.) gauge length, and Charpy V-notch (CVN) impact specimens were machined from the concast rods, simulated sand-cast rods and modified keel blocks.

2.2 CORROSION INHIBITING HEAT TREATMENT

Zanis (5) and others have shown that, under certain conditions, heat treatment for 6 h at 700°C followed by air cooling, will reduce or eliminate the $\alpha + \gamma_2$ structure which is highly susceptible to corrosion attack. This heat treatment is now mandatory in MIL-B-24480 (Ships) 1973. Accordingly, the heat treatment was applied to many of the compositions in this study, and the effects on the mechanical properties and microstructure of concast, simulated sand-cast and sand-cast alloys were investigated. The effect of heat treatment at 600 and 650°C was also investigated.

2.3 ELECTRON MICROSCOPY

Specimens for electron microscopy were mechanically polished on 600-grit emery paper followed by electropolishing in a 50% orthophosphoric acid solution to about 0.13 mm (0.005 in.). Disc specimens of 3 mm diam were spark cut, and final polishing was carried out in a twin-jet electro-polisher using a solution containing 25% conc. nitric acid and 75% methanol at a temperature of -20 to -25°C. Specimens were observed in a 100kV Phillips Em300 electron microscope which has an energy dispersive analyzer.

2.4 WELDING

The chemical compositions of alloys used for restrained butt weld tests are listed in Table 4. Melt quality was assessed from tensile and impact tests carried out on specimens cut from modified keel blocks poured at the same time. Sand-cast plates, 25 x 152 x 305 mm (1 x 6 x 12 in.) with a 30° bevel on one 305 mm (12 in.) side, were examined by radiography. A backing strip approximately 10 x 25 mm (3/8 x 1 in.) was cut from the non-bevelled edge of a plate for use in making each assembly of two plates. All the backing strips were radiographed also, to assess their soundness. Welding was carried out using commercial 1.6 mm (1/16 in.) "Ampcotrode 46" and Ampcotrode 10" filler wires and a low aluminum filler wire made in this laboratory. The chemical compositions of these wires are shown in Table 5.

The low-aluminum (8.5% Al) filler wire was produced from 22 mm (7/8 in.) diameter concast rods by hot swaging and wire drawing with intermittent annealing and pickling.

The first five passes of welds made by buttering techniques were made with Ampcotrode 10 filler wire and the last five passes with Ampcotrode 46.

Welds were made using the welding jig shown in Fig. 1. Prior to assembly, the bevelled surfaces of the cast plates, including the upper surface of the backing strip, were ground (with a hand-held power grinder), degreased and finally cleaned with suitable solvents. The test plates were mounted so that the outer edge of one plate was offset by about 5 mm (3/16 in.) from the other plate to compensate for distortion. Run-on and run-off blocks (cut from NAB castings) were used with the same joint configuration as the test plates.

Table 6 gives the joint design and the welding parameters for the GMAW tests. In accordance with Canadian DG ships specifications (6), the filler wire was fed through a piece of lint-free cloth to maintain cleanliness. Considerable care was taken following each bead to remove all the oxidized surfaces, irregularities or sharp re-entrant angles at the edge of the bead by grinding or wire brushing. This was done to prevent any difficulty in obtaining good fusion when the next bead was deposited.

Each weld was sectioned after radiographic and dye-penetrant inspection, to provide 2-4 transverse side bend coupons of 10 x 22 x 152 mm (3/8 x 7/8 x 6 in.), at least one metallographic specimen, 2-4 transverse tensile specimens of 13 mm (0.505 in.) diam, and 2 Charpy V-notch (CVN) impact specimens from the soundest locations. Steps were taken to ensure that welds were located in the gauge section of tensile specimens and at the centre of bend specimens. Similarly, the V-notch of the Charpy specimens was machined in the fusion-zone of welds. Metallography, and bend, tensile and impact tests were carried out on specimens in both as-welded and post-weld heat treated (700°C, 6 h, air cooled) conditions.

In performing bend tests, coupons were bent around a 38 mm (1 1/2 in.) diam mandrel (corresponding to 2 T bend radius, where T is the specimen thickness), until 180 degrees was attained or the coupons cracked to a greater length than 3 mm (1/8 in.).

3. RESULTS AND DISCUSSION

3.1 CONCAST MATERIALS

3.1.1 Mechanical Properties

Tensile and impact properties for the concast, and concast and heat treated conditions are summarized in Table 2 and Figs. 2 to 4. Various ways of plotting strengths as a function of a compositional parameter (e.g., Ni, Fe, Ni:Fe ratio, Al + Ni, etc.,) were explored, with the only siginificant relations being those shown in Fig. 2 vs. aluminum content. As shown, both yield and ultimate strength increase with aluminum content at the rate of 124 and 172 MPa (18 and 25 ksi) per wt % Al respectively. Note that the data in Fig. 2 include all nickel, iron and aluminum levels. All compositions above 8.25% Al exceed the tensile strength requirements of ASTM B505 (alloy C95800) with combinations of 414 MPa (60 ksi) yield and 758 MPa (110 ksi) ultimate strengths at high aluminum levels (9.5% Al).

For aluminum contents of less than 9.2%, the 700°C heat treatment increases both yield and ultimate strengths, the percentage increase diminishing from 25 to 30% at 8.1% Al to zero per cent at 9.2% Al. In all alloys containing >9.2% Al, heat treatment reduced tensile strength values.

The ductility data in Table 2 and Fig. 3 show an expected reduction in tensile elongation with increase in aluminum content in the as-cast condition, with the specified minimum being exceeded for most compositions containing <9.2% Al. Most compositions displayed ductilities in the range of 15 to 25% after heat treatment.

Charpy V-notch fracture energies at room temperature for all as-cast alloys are plotted in Fig. 4 against aluminum content. Again, the aluminum content was the only meaningful compositional parameter found. The high impact properties of the continuously cast stock are reduced to ~27 J (~20 ft-lb) by the 700°C heat treatment below 9.3% Al.

Density measurements were made on all continuously cast products to confirm their freedom from porosity. The data show a strong correlation with aluminum content, irrespective of the levels of iron, nickel and manganese (Fig. 5).

3.1.2 Precipitation Strengthening Effects of Heat Treatment

To further illustrate the increase in strength caused by heat treatment, selected alloys in the range 8.44 to 9.87% Al, were hardness tested at room temperature after a 3 h anneal at 250-750°C. Figure 6 illustrates the hardening response obtained with peak hardnesses occurring at lower temperatures as the aluminum content of the alloys increases. The compositions examined had Ni:Fe rations of ~1. The highest response obtained was for alloy CA12-2 (8.75% Al), "aged" at 650°C for 3 h.

The more conventional type of precipitation hardening relationship is illustrated in Fig. 7 for alloy CA7-1 (8.44% Al, 4.30% Ni, 4.28% Fe, 1.21% Mn). Hardness at room temperature after precipitation "ageing" for various times at each of three temperatures is plotted as a function of time. It should be noted that the heat treatments at 600, 650 and 700°C were carried out on samples originally in the as-cast condition, i.e., as-continuously cast. No high-temperature solution heat treatment was performed prior to these medium temperature ageing treatments. The results indicate that for this one composition at least, the specified 700°C for 6 h "corrosion inhibiting heat treatment" produces a slightly overaged condition, and that the lower heat treatment temperatures of 600°C and 650°C produced higher hardening maxima than were obtained at 700°C. It was confirmed for a number of compositions that this higher hardening response at lower temperatures reflects a greater degree of precipitation strengthening. Tensile specimens of selected alloys were heat treated at 650°C for 6 h, their properties being compared in Table 8 with their as-cast and 700°C treatment values. In all cases, the lower heat treatment temperature of 650°C resulted in significant increases in yield strength over those values obtained at 700°C.

3.1.3 Microstructures

The secondary phases in these continuously cast alloys are irresolvable at a magnification of 1000 in an optical microscope [Fig. 8 (a) and (b)]. Examination by scanning electron microscopy at a magnification of 5000 (Fig. 9) presented a more detailed illustration of the phases originating from the high-temperature β phase. In the as-cast condition, it is seen that even at low aluminum levels of ~8%, the α + κ eutectoid contains dark irresolvable areas which, in the more massive secondary phases of sand-cast material, have been identified as $\alpha + \gamma_2$. The volume fraction of β-from which α + κ phases

originate increases with aluminium level, as does the volume of $\alpha + \gamma_2$ inside those regions. The primary α is relatively precipitate-free in all four sections.

Massive precipitation in the α phase and a spheroidization, or break-up, of the lamellar κ constituent in the as-cast structure is induced by heating these cast structures to 700°C and holding there for 6 h, followed by air-cooling. Simultaneously, the aluminum-rich γ_2 phase is eliminated from the microstructure. Figure 10 compares cast, and cast and heat treated microstructures for three alloy compositions varying only in aluminum content (Ni:Fe ratio = 1). A preliminary analysis of the precipitated phase by X-ray dispersive techniques indicated on the basis of composition only, the precipitate was one of the continuous series of κ solid solutions, containing, in this case, equal amounts of iron and nickel. The lower heat treatment temperature of 650°C also eliminated γ_2 from the microstructure in the few samples examined.

3.2 SIMULATED AND SAND-CAST MATERIAL

3.2.1 Structure and Properties - As-cast Condition

The original continuous cast microstructure consists of dark etching $\alpha + \gamma_2$ (decomposed β) in α matrix. The β phase is reformed on homogenizing at 1000°C and the iron-rich or nickel-rich κ is precipitated in the manner previously discussed (2), the remaining β transforming to $\alpha + \gamma_2$. The same reactions take place as the sand casting cools from the solidification temperature through 1000°C to room temperature.

The microstructures of simulated sand-cast material and actual sand-cast material from a similar composition are shown in Fig. 11. Both structures show "globular" iron-rich and "lamellar" nickel-rich κ, and dark etching $\alpha + \gamma_2$ formed from the last of the β phase. It may be noted that the κ precipitates within the α phase are somewhat coarser in the simulated material, probably because the cooling rate between say, 800 and 500°C was slower than the cooling rate of the sand-cast keel blocks in this temperature range.

This similarity in microstructures is also reflected in the mechanical properties as shown in Fig. 12 and Tables 3 and 8, which also indicate the minimum mechanical property requirements of ASTM B148 for this alloy. The slightly higher properties of the simulated material may be due to its greater homogeneity.

It will be seen that practically all the material meets the UTS and percentage elongation requirements, but the YS is met only when the aluminum content exceeds 9.5%. No strong effect of Ni:Fe ratio was apparent. However, slightly better toughness (El% and Charpy impact) was obtained at low Ni:Fe ratios.

3.2.2 Structure and Properties - Heat Treated Condition

Previous work (2) has shown that the effect of 700°C, 6 h heat treatment is to reform the β phase from the room temperature $\alpha + \gamma_2$ phase; at 700°C β may disappear, or may transform to $\alpha + \kappa$, but both transformations are diffusional processes as the system moves towards equilibrium. It should be noted that at lower temperatures the reaction time is increased, whereas at higher temperatures there is progressively more β in the equilibrium structure which might be retained to re-transform to $\alpha + \gamma_2$ on cooling through the 565°C transformation temperature.

Figure 13 shows the microstructures of both simulated and sand-cast materials after 6 h at 700°C followed by air cooling. By comparison with Fig. 11, it will be seen that the $\alpha + \gamma_2$ has been completely eliminated, and although precipitation has been induced in the α phase of both, the effect is much more pronounced in the sand-cast materials. This is shown in greater detail in the scanning electron micrographs of Fig. 14 and 15.

The observed changes in microstructure are reflected in corresponding changes in mechanical properties and, as shown in Fig. 16, the majority of the material now meets the mechanical property requirements. The properties of both simulated and sand-cast materials before and after the corrosion-inhibiting heat treatment are illustrated in Fig. 17 which shows:

a) a significantly greater response to heat treatment in the sand-cast materials,

b) a very useful increase in yield strength in the heat-treated sand-cast material, particularly at the low aluminum levels, and

c) after heat treatment, the yield strength and elongation values of the sand-cast material are relatively independent of aluminum content.

The "plateau" shown for the elongation values of the simulated material is somewhat suspect because corresponding Charpy impact values show a steady decline with increasing aluminum content, as shown in Fig. 18.

It is apparent from this that more than solution and diffusion takes place as $\alpha + \gamma_2$, is removed during the corrosion inhibiting treatment but that significant precipitation hardening also takes occurs.

3.2.3 Impact Properties

Although, Thomson (18) has investigated the effect of test temperature on the impact properties of sand-cast NAB alloys over a wide range of compositions, none of his alloys matched the nominal compositions in Table 1. Thus, it was of interest to obtain a more complete picture of the impact energies for both as-cast, and cast and heat treated material.

Charpy V-notch fracture energies measured at room temperature for the as-cast, and as-cast and heat-treated conditions are plotted in Fig. 18 against aluminum content. The impact properties of simulated alloys, are also replotted in this figure for comparison. Figure 18 shows that above 9.5% Al, the impact energies of both sand-cast, and sand-cast and heat-treated alloys are about 27 J (20 ft-lb), which is a reasonable value for most applications. The impact energies of both sand-cast, and simulated sand-cast alloys are reduced by the 700°C heat treatment below 9.5% Al. It is interesting to note that an impact energy of about 32 J (24 ft-lb) can be expected in alloys containing about 8.5% Al, even after the 700°C heat treatment.

Figure 19 shows the influence of test temperature on the impact properties of concast, simulated sand-cast, and sand-cast alloys in both the as-cast, and the as-cast and heat-treated conditions. The effect on the impact properties at various test temperatures of increasing the aluminum content of sand-cast alloys is illustrated in Fig. 20. Figures 19 and 20 show that for every alloy, the impact toughness for the heat-treated condition is less than that in the as-cast condition. No sharp temperature transitions in impact toughness are observed. Instead, impact toughness gradually declines with decreasing temperature, but at room temperature, all materials have CVN values in excess of 27 J (20 ft-lb).

3.2.4 Precipitation Hardening Effects of Heat Treatment

Simulated and sand-cast specimens containing about 8.25% Al, 4.5% Fe and Ni, and 1.1% Mn were heat treated at 600, 650, and 700°C for various times up to 8 h to further investigate the precipitation effects. The results of hardness tests, plotted in Fig. 21, again show the greater response of the sand-cast material, and also show that the highest hardness is obtained at the lowest temperature, and that the recommended 6 h treatment at 700°C overages both materials.

Tensile, impact and hardness tests on sand-cast materials (melt #2252, 8.65% Al, 4.47% Ni, 4.33% Fe and 0.86% Mn), aged for 6 h at temperatures between 450 and 750°C shows that peak strengthening occurs at 600°C (Fig. 22).

Additional microhardness testing indicated that the α phase in the simulated material was already at peak hardness, and hence did not further harden on heat treatment. In contrast, heat treating the sand-cast material increased the hardness of the α phase to the level already attained by the simulated material. It was also shown that the hardness was independent of the cooling rate from the heat treating temperature, and that overageing occurs more rapidly and at lower temperatures as the aluminum content increases.

3.2.5 The Effect of Composition on the Occurence of γ_2 and its Subsequent Removal by Heat Treatment

It is known that manganese, like aluminum, increases the amount of β in the structure, and it is said to "stabilize" the β, leading to the retention of $\alpha + \gamma_2$ in the room temperature microstructures (5). To minimize retention, Zanis and Ferrara recommend that manganese be reduced from 3.5% maximum to the present 1.5% maximum in alloy C95800 and that a heat treatment be applied to remove the γ_2 (5).

All the materials in the present investigation were examined for the presence of dark etching $\alpha + \gamma_2$ and some results are given in Tables 3 and 8. It was shown that γ_2 occurred at approximately the same compositions and under the same conditions, in both the sand-cast and the simulated material. This suggests that segregation during solidification need not be considered, as the continuously-cast simulated material should be considerably more homogeneous than the sand-cast material in the distribution of aluminum or manganese, for example.

All the results are summarized in Table 9 which shows the values of aluminum and manganese at which γ_2 is present in the as-cast or simulated material, and the limitations on γ_2 removal by the 6 h, 700°C corrosion-inhibiting heat treatment.

It should be noted that in marginal cases where the γ_2 is not completely removed by the heat treatment there still may be substantial improvement in corrosion resistance once the $\alpha + \gamma_2$ islands become so small they no longer form a continuous network in the structure.

3.3 PHASE ANALYSIS

The various phases present in the complex NAB alloys are the α matrix, γ_2 (whose presence is determined by Al and Mn contents) and κ, which is the product of the eutectoidal transformation of the β phase

$$\beta \rightarrow \alpha + \kappa \qquad \ldots.(1)$$

The various forms of κ phase for alloy 2086-3 (8.98% Al, Ni:Fe ratio of 1.2) are identified in Fig. 23 using the terminology of Weill-Couly and Arnaud (19). They are designated as follows:

κ_I → large particles of propeller or rosette form, thought to be iron-rich,

κ_{II} → smaller cruciform phase, thought to be iron-rich,

κ_{III} → lamellar or lath-shaped, thought to be nickel-rich,

κ_{IV} → fine precipitates in α grains, thought to be iron-rich.

Thomson and Edwards (2) have shown that κ phase is stable over a wide temperature range and Fe and Ni composition limits and that its precipitation mode and subsequent morphology are determined by the Fe and Ni concentrations. They described the nodular form of the κ phase as Fe-κ, and the lamellar, or lath-shaped form as Ni-κ.

In the past, analytical electron microscopy of thin foils and extraction replicas, together with scanning electron microscopy of bulk specimens have been used to determine the composition of the various forms of κ phase (20,21). However, the morphology and composition of the phases precipitated during a corrosion inhibiting heat treatment have not been studied in detail. The aim of the present investigation was to use transmission electron microscopy to characterize the phases present in a typical sand-cast alloy

(2086-3) in both the cast and 700°C heat treated conditions, and to identify the composition of the phases by energy dispersive analysis.

Quantitative analysis of the phases was carried out by a technique developed by Cliff and Lorimer (22). In this method, X-ray intensities of two elements can be measured simultaneously (at constant kilovoltage and moderate specimen thickness). Thus

$$\frac{C_1}{C_2} = \frac{k_1 I_1}{k_2 I_2} \qquad \ldots.(2)$$

where C_1 and C_2 are the concentrations (wt%) of two elements, k_1 and k_2 are tensity correction factors for the two elements, and I_1 and I_2 are inchar-acteristic X-ray intensities for each element.

The k values can be calculated (23), or preferably, determined experimentally (21,22) by analyzing standards of known chemical composition. In the present investigation, k values determined experimentally by Culpan and Rose (21) were used. These values resulted in precipitate analyses in as-cast samples that agreed reasonably well with similar analyses by other workers (20,21). However, it may be noted that the k values may change from instrument to instrument because the EDS detector and the specimen environments are not the same on all instruments.

Figures 24 and 25 are transmission electron micrographs of sand-cast alloy 2086-3 (8.98% Al, 4.74% Ni and 3.93% Fe) showing the morphology of the κ_{III} and κ_{IV} phases respectively. Figure 25 also shows an unidentified finely dispersed phase in the α grains.

Figure 26 is an electron micrograph of the 700°C heat treated alloy showing the phases precipitated in the α matrix. These precipitates are found to be of two distinct forms. One type is usually spherical or barrel-shaped and approximately one μm in diam. The second is in the form of short platelets (approximately 1μm X 2μm). It will be seen that the morphology of these new phases is markedly different from that found in the sand-cast structure (cf. Fig. 25).

The average chemical analysis of some of the phases found in sand-cast, and cast and heat-treated NAB alloys is given in Table 10. For comparison, the chemical analyses reported by other workers are also included.

Table 10 shows that the chemical compositions determined in the present work are similar to those reported by others (21,22).

Table 10 also shows that the spherical or barrel-shaped precipitates that form during the corrosion-inhibiting heat treatment are iron-rich, whereas the platelets are rich in Ni, Al and Cu. It will be seen that the compositions of these low temperature spherical or barrel-shaped precipitates and the platelets are similar to those of the high temperature κ_{II} and κ_{III} phases respectively.

3.4 WELDABILITY

3.4.1 Welding Characteristics and Weld Soundness

The welding characteristics of NAB alloys have been investigated by a number of workers and procedures for weld repairing have also been described (6,25-30). In the present work it was observed during trial runs, that welding with pure argon as a shroud produced excessive porosity throughout the weld, with some pores up to 1 mm in diam. However, sound welds were produced when a mixture of argon and helium (up to 15% He) was used instead. Although porosity-free welds were readily obtained, lack of penetration or fusion and oxide inclusions occurred in some welds when high aluminum (>9.25% Al) filler wires were used. In such welds, the spray transfer obtained in the first 2-3 passes degenerated to sputtering despite variation of the interpass temperature between room temperature and 180°C. Although only one weld was made with the new low-aluminum filler wire, its welding characteristics were judged to be superior to the rest.

It may be noted that weld-toe cracks observed in GMA welds of both Nb and Cr-modified 70/30 Cu-Ni alloys (31), did not occur in NAB welds. No HAZ cracking was detected.

3.4.2 Metallography of GMA Welds

Figure 27, the macrostructure of weld 2057-2, is typical of all welds. Metallographic examination revealed a narrow (about 0.8 mm wide) heat-affected zone (HAZ). Figures 28(a) to (f) show the narrow HAZ of welds made with different filler wires on parent metal with various aluminum contents. In these optical micrographs, the acicularity of the fusion zone microstructure is more pronounced in welds made with filler wires of higher aluminum content.

Scanning electron microscopy (SEM) was used where the fine microstructural features of the fusion zone and HAZ could not be resolved optically. Figures 29 and 30 show that, in the un-heat-treated condition, the fusion zone and HAZ of welds made with Ampcotrode 46 and the new low aluminum filler wires consists of fine κ phases and the dark etching γ_2 phase embedded in an α matrix - the volume fraction of the γ_2 phase being low in welds made with the low aluminum filler wire. The similarity oetween these microstructures and those of concast and permanent mould cast NAB alloys (7,32) implies that the HAZ near the fusion line (F/L) is heated to about 950-1000°C (high temperature β phase region) and that subsequent rapid cooling produces fine κ and γ_2 phases. No significant changes in the microstructure were observed except for the presence of globular κ in α at distances of about 0.5 mm from the F/L, where the temperature is less than 800°C.

Post-weld heat treatment (6 h at 700°C) induces copious precipitation of fine κ phases in the α matrix and spheroidization of lamellar constituents in the fusion zone and HAZ, coupled with complete solution of any γ_2 phase (Figs. 31 and 32). It is interesting to note that in the as-welded condition, the $\alpha + \gamma_2$ structure is observed in the HAZ of the parent metal containing very low aluminum (~8.25% Al). However, following the 700°C heat treatment, there are no significant differences in the microstructures of the HAZ of welds made with various aluminum contents, although the volume fraction of the spheroidized phases increases as the aluminum content of the base metal increases.

The microstructural features of the base metal have been described in detail in section 3.2.1 and 3.2.2.

In the case of weld 2156-2, welded with Ampcotrode 46 filler wire, the base plates had been heat treated at 700°C for 6 h prior to butt welding. Thus, there was already abundant precipitation of the fine κ phases in the α phase. Despite this, the microstructure of the HAZ was similar to that described above and exhibited the $\alpha + \gamma_2$ structure. Following the post-weld heat treatment, a microstructure, similar to that described earlier, was produced in the fusion zone and HAZ (Fig. 32(b) and (c)). However, coarsening of the κ phases in the α phase of the base metal took place because of the second 700°C heat treatment.

The HAZ microstructure of welds made with Ampcotrode 10 filler wire is similar to the microstructure of welds made with Ampcotrode 46 filler wire. However, the microstructure of the fusion zone is different because of the difference in composition of the filler wire. In the case of Ampcotrode 10, the fusion zone microstructure, in the as-welded condition [Fig. 33(a) and (b)] is predominantly β with some fine κ phases in both the α and β fields. Following the post-weld heat treatment, the microstructure of the fusion zone, 2-4 mm away from the fusion line, did not break down completely [Fig. 33(c)]. However, near the fusion line, there was copious precipitation of the spherical and lath shaped iron-rich κ phases [Fig. 33(d)] in the α matrix, probably because of the diffusion of aluminum from the fusion zone to the base metal during the 700°C, 6 h heat treatment. The diffusion distance for the aluminum-depleted zone inside the fusion zone varies from 0.5 mm to 3 mm.

Optical micrographs of the transition zone between the Ampcotrode 10 and 46 filler wires for welds made by the buttering technique are shown in Fig. 34 (a) and (b) for the as-welded condition. There is no significant change in the microstructure of the fusion zone of the last pass of the Ampcotrode 10 from the heat received from the Ampcotrode 46 deposits. After the post-weld heat treatment, the microstructures of the fusion zone for the two filler wires are modified as described earlier, and there appears to be diffusion of aluminum from the Ampcotrode 10 zone to both the base metal and the Ampcotrode 46 zone; the diffusion distance for the aluminum-depleted zone being about 0.1 mm for Ampcotrode 10 and 0.05 mm for Ampcotrode 46 (Figs. 34(c) and (d)).

3.4.3 Mechanical Properties

Tensile and impact properties of the sand-cast, and sand-cast and heat-treated (700°C, 6 h) alloys, obtained from modified keel blocks and/or welding plates, are presented in Table 4. The properties are consistent with the data reported earlier i.e. with increasing aluminum content the UTS and YS increase and the % elongation and CVN impact properties decrease. The mechanical properties of the modified keel block did not differ significantly from those obtained from the 25 x 152 x 305 mm (1 x 6 x 12 in.) plate castings.

Transverse-weld tensile and impact properties of the as-welded and post-weld heat treated specimens are summarized in Table 11, and plotted in Fig. 35 as a function of aluminum content. With the exception of weldments prepared using Ampcotrode 10 filler wire, which gave rise to oxidation defects in the weld, all the welds were stronger than the parent metal (Tables 4 and 11). Therefore, tensile tests of sound specimens in the as-welded condition mirror the properties of the as-cast material. Conversely, the CVN impact properties are those of sound weld material because the fracture is forced to propagate through the weld by the specimen configuration. Similar conclusions can be drawn for specimens tested in the post-weld heat treated condition.

Heat treatment of the base metal at 700°C prior to constrained butt welding caused significant increases in the yield strengths of the welded specimens consistent with the expected increase in strength of the base metal. However, UTS and elongation values could not be determined because of the presence of oxidized defects in the gauge section. Post-weld heat treatment of this sample at 700°C decreases the yield strength probably due to overaging of the parent metal.

Note that the experimental low-aluminum filler wire gives the highest RT CVN impact values, apart from the nickel-free Ampcotrode 10 filler wire.

SUMMARY AND CONCLUSIONS

1. The precipitation hardening response of continuously cast nickel-aluminum bronze has been determined for a number of compositional variitions, and the mechanical properties of both cast and heat-treated materials have been shown to meet the ASTM B505 specification for alloy C95800, provided the aluminum level in the alloy is less than 9.2%.

2. It is suggested the standard corrosion-inhibiting heat treatment of 700°C for 6 h is not the optimum for precipitation strengthening. The data indicate that a lower temperature of 650°C for a period of 12 to 20 h will further improve strength properties while simultaneously eliminating γ_2 microsegregation from the continuously cast product.

3. It is possible to simulate the structure and properties of sand-cast material by making continuously cast rods, heat treating them at 1000°C, then slow cooling them. This method has proved to be a most convenient experimental tool.

4. The complete or partial removal of the deleterious γ_2 phase was observed after the recommended corrosion-inhibiting heat treatment (700°C for 6 h followed by air cooling), and the critical aluminum and manganese contents for complete removal of γ_2 have been documented.

5. This heat treatment also causes marked precipitation of fine κ within the α phase with significant increase in strength and reduction in ductility. These effects are less pronounced in the simulated material produced by continuous casting than in sand-cast material probably because the prior heat treatment causes similar precipitation.

6. It is shown that the effect of this precipitation on mechanical properties is greatest at low aluminum contents (<8.75%) and that even greater increases in strength could be obtained by reducing the time or temperature of heat treatment. However, such conditions detract from the elimination of γ_2 from the microstructure.

7. In the sand-cast condition only one composition $\geq$9.25% Al met all the mechanical property requirements of ASTM B148 for alloy C95800, but after the 700°C heat treatment substantially all the material, even with as little as 8.0% Al, met these requirements.

8. Two types of phases are precipitated during the corrosion-inhibiting heat treatment. One is spherical or barrel-shaped, and the other has a plate-shaped morphology. The former is found to be an iron-rich phase, whereas the latter is rich in Ni, Al and Cu.

9. Porosity-free welds can be obtained by using 15% argon-helium mixtures as a shroud.

10. High-aluminum filler wires are likely to produce oxide inclusions in the weld.

11. The deleterious γ_2 phase is formed in the HAZ of welds irrespective of the filler wire used. In the case of the Ni-Al bronze filler wires, γ_2 phase is also present in the fusion zone.

12. The post-weld heat treatment at 700°C for 6 h eliminates the γ_2 phase from the fusion zone and HAZ, and causes spheroidization of the κ phases in both regions.

13. The UTS and YS properties are increased and the elongation and CVN impact values are reduced by the post-weld heat treatment, especially at the low aluminum end of the composition range.

14. Weld repairing by the "buttering" technique using two filler wires (nickel-free high aluminum and complex nickel-aluminum bronze) is not recommended.

15. Current philosophy is to select an alloy of relatively high aluminum content to meet the mechanical properties and then heat treat to remove the γ_2 phase, thus improving the corrosion resistance. The present work suggests it would be better to choose an alloy of lower aluminum content, say 8.5% Al, which should contain little or no γ_2 phase and hence should have inherently good corrosion resistance. These castings should be welded or weld-repaired with filler wire of matching composition. The post-weld heat treatment can then be employed to remove the γ_2 phase from the fusion zone and HAZ and to improve the mechanical properties of the casting.

ACKNOWLEDGEMENTS

The author is indebted to Mr. J.O. Edwards, formerly Head, Non-Ferrous Metals Section (retired), for his advice and comments on various aspects of Ni-Al bronze alloys. Special thanks are extended to Mr. R. Hoare for his patience in doing all the MIG welding. The author also acknowledges the help received from the following: the foundry support staff for their help in melting and casting; Messrs. J.R, Barry and K. Kleinschmidt for the expert assistance in heat treatment and metallography; Mr. G. Weatherall for mechanical testing; Mr. M. Charest for transmission electron microscopy; Mr. V. Chartrand for scanning electron microscopy, the Mineral Sciences Lab for chemical analysis; and Mr. H.P. Guindon for continuous casting.

REFERENCES

1. Thomson, R. and Edwards, J.O. "Effect of Compositional and Process Variables on the Tensile Properties of Cast Nickel-Aluminum Bronze", AFS Transactions, vol. 85, p.13 (1977)

2. Thomson, R. and Edwards, J.O. "The Kappa Phase in Nickel-Aluminum Bronze, Part I: Slow-Cooled Microstructure", AFS Transaction, vol. 86, p. 385 (1978)

3. Thomson, R. and Edwards, J.O. "The Kappa Phase in Nickel-Aluminum Bronze, Part II: Cast Microstructures and Properties", AFS Transactions, vol. 86, p. 395 (1978)

4. Zanis, C.A. and Ferrara, R.J. "An Investigation into Dealloying of Cast Ni-Al Bronze", AFS Transactions, vol. 80, p. 259 (1972)

5. Zanis, C.A. and Ferrara, R.J. "Sea Water Corrosion of Nickel-Aluminum Bronze", AFS Transactions, vol. 82, p. 71 (1974)

6. "Proposed Specifications DG Ships/PS/9011A, Welding of Copper Based Alloy Castings", Ministry of Defence, U.K. (1974)

7. Thomson, R. and Sahoo, M. "The Structure and Mechanical Properties of Continuously Cast Ni-Al Bronze Bar Stock", AFS Transactions, vol. 87, p. 485 (1979)

8. Sahoo, M., Edwards, J.O. and Thomson, R. "Influence of Corrosion Inhibiting Heat Treatment on the Microstructure and Mechanical Properties of Nickel-Aluminum Bronze Alloy C95800", AFS Transactions, vol. 87, p. 495 (1979)

9. Sahoo, M., Edwards, J.O. and Thomson, R. "Influence of Corrosion-Inhibiting Heat Treatment on the Microstructure and Impact Properties of Nickel-Aluminum Bronze Alloy C95800", AFS Transactions, vol. 88, p. 769 (1980)

10. Sahoo, M. Barry, J.R. and Kleinschmidt, K. "Use of Ceramic Foam Filters in the Brass and Bronze Foundry", AFS Transactions, vol. 89, p. 611 (1981)

11. Sahoo, M. "Weldability of Nickel-Aluminum Bronze Alloy C95800". Lab Report MRP/PMRL 81-83 (OP-J), CANMET, Energy, Mines and Resources, Canada; (1981)

12. Sahoo, M. "High-Strength Copper Base Alloys for Shipboard Systems. Nickel-Aluminum Bronze Alloys: Progress Report No. NAB-3, October 1 - December 31, 1978"; Lab Report MRP/PMRL 79-9 (TR); CANMET, Energy, Mines and Resources, Canada; (1979)

13. Idem, ibid, Progress Report No. NAB-4, January 1 - March 31, 1979. Lab Report MRP/PMRL 79-41 (TR); CANMET, Energy, Mines and Resources, Canada; (1979)

14. Idem, ibid, Progress Report No. NAB-5, April 1 - June 30, 1979. Lab Report MRP/PMRL 79-51(TR); CANMET, Energy, Mines and Resources Canada; (1979)

15. Idem, ibid, Progress Report No. NAB-6, July 1 - September 30, 1979. Lab Report MRP/PMRL 79-75 (TR); CANMET, Energy, Mines and Resources, Canada; (1979)

16. Idem, ibid, Progress Report No. NAB-7, October 1 - December 30, 1979. Lab Report MRP/PMRL 80-14 (TR); CANMET, Energy, Mines and Resources, Canada; (1980)

17. Sahoo, M., Barry, J. and Kleinschmidt, K. Ibid, Progress Report No. NAB-8, January 1 - June 30, 1980. Lab Report MRP/PMRL 80-53 (TR); CANMET, Energy, Mines and Resources, Canada; (1980)

18. Thomson, R. "Charpy Impact Properties of Bronze Propeller Alloys", AFS Transactions, vol. 76, p. 189 (1968)

19. Weill-Couly, P. and Arnaud, D. "Effects of Composition and Structure of Aluminum Bronzes on their Service Performance", AFS Transactions, vol. 86, p. 385 (1978)

20. Lloyd, D., Lorimer, G.W. and Ridley, N. "Characterization of Phases in a Nickel-Aluminum Bronze", Metals Technology, vol. 7, p. 114 (1980)

21. Culpan, E.A. and Rose, G. "Microstructural Characterization of Cast Nickel-Aluminum Bronze", J. of Materials Science, vol. 13, p. 1647 (1978)

22. Cliff, G. and Lorimer, G.W. "The Quantiative Analysis of Thin Specimens" J. of Microscopy, vol. 103 (Part 2), p. 203 (1975)

23. Goldsteing, J.I., Costley, J.L., Lorimer, G.W. and Reed, S.J.B. "Quantitative X-ray Analysis in the Electron Microscope", Proc of the Workshop in Analytical Electron Microscopy, SEM, vol. 1, IIT Research Institute, Chicago, p. 315 (1977)

24. Thomson, R. and Dion, J.L. "Complex Aluminum Bronzes. Part V: The Analysis of Secondary Phases in Aluminum Bronze Containing Iron and Nickel", Internal Report PM-R-67-2, Physical Metallurgy Division, Energy, Mines and Resources, Canada (1967)

25. Wilson, C.V. "Welding of Aluminum Bronze - I", Metal Industry, vol. 104, p. 316 (1964)

26. Wilson, C.V. "Welding of Aluminum Bronze - II", Metal Industry, vol. 104, p. 348 (1964)

27. Clews, K.J. "Metallurgical Aspects of Aluminum Bronze Welding Problems", British Welding Journal, vol. 12, p. 126 (1965)

28. Clews, K.J. and Battarbee, W.F.J. "Welding Repair of Aluminum Bronze Castings to BS 1400-AB2C", BWRA Reasarch Report No. C152/2/67, February 1967

29. Dimbylow, C.S. and Dawson, R.J.C. "Assessing the Weldability of Copper Alloys", Weld Metal Fabrication, vol. 46, p. 461 (Sept. 1978)

30. "Welding Handbook, Copper and Copper Alloys", American Welding Society, 1972. Distributed by Canadian Copper and Brass Development Association, Toronto.

31. Sahoo, M. and Campbell, W.P. "Weldability of Both Nb-Modified and Cr-Modified High-Strength Cu-Ni Casting Alloys", AFS Transactions, vol. 88, p. 727 (1980)

32. Whiting, L.V., Sahoo, M. and Brown, D.A. "Structure and Mechanical Properties of Aluminum Bronze Alloys Cast in the ISO Permanent Test-Bar Mould", AFS Transactions, vol. 89, p. 659 (1981)

Table 1. Alloying ranges in continuously cast nickel-aluminum bronzes

	Nominal wt %	Actual wt %
Nickel - 1 level	4.5	4.01 - 4.6
Iron - 3 levels	3.5	
	4.5	2.96 - 5.13
	5.0	
Manganese - 2 levels	0.8	0.65 - 1.26
	1.3	
Aluminum - 3 levels	8.25	
	8.75	8.09 - 9.9
	9.25	

Table 2. Chemical compositions and mechanical properties of concast rods, (7/8-in. 22-mm diam.)

Composition, wt %						Mechanical Properties							
						Concast				Concast + 700°C 6 h, air cooled			
Sample No.	Ni	Fe	Al	Mn	Ni/Fe Ratio	UTS ksi (MPa)	0.5% YS, ksi (MPa)	El% on 2 in. (51 mm)	Charpy impact ft-lb (J)	UTS YS, (MPa)	0.5% YS, ksi (MPa)	El% on 2 in. (51 mm)	Charpy impact ft-lb (J)
CA 1-1	4.22	3.85	8.48	0.96	1.1	87.6 (604)	38.2 (263)	31.5	45.7 (62)	92.3 (636)	43.2 (298)	19.0	17.7 (24)
CA 1-2	4.17	4.33	9.17	1.12	1.0	100.7 (694)	53.2 (366)	13.0	18.4 (25)	103.1 (710)	53.0 (365)	20.0	18.4 (25)
CA 1-3	4.01	4.50	9.60	1.16	0.9	110.6 (762)	69.6 (479)	7.0	11.1 (15)	106.6 (734)	63.5 (437)	17.0	15.5 (21)
CA 2-1	4.18	4.84	8.45	0.86	0.9	88.5 (610)	38.8 (267)	33.5	47.9 (65)	92.9 (640)	45.5 (313)	15.0	19.9 (27)
CA 2-2	4.15	4.91	8.96	0.86	0.8	100.3 (691)	46.7 (322)	23.5	31.0 (42)	103.0 (710)	50.0 (344)	20.0	18.4 (25)
CA 2-3	4.14	4.84	9.13	0.86	0.8	108.5 (748)	51.2 (353)	19.0	21.4 (29)	104.3 (719)	51.2 (353)	21.5	18.4 (25)
CA 3-1	4.29	4.08	8.58	1.24	1.0	86.4 (595)	39.7 (273)	36.0	47.9 (65)	95.4 (657)	45.0 (310)	20.0	19.9 (27)
CA 3-2	4.30	4.58	8.88	1.24	0.9	96.5 (665)	46.8 (322)	27.0	37.6 (51)	103.3 (712)	52.0 (358)	20.5	19.9 (27)
CA 3-3	4.44	4.39	9.33	1.22	1.0	106.9 (736)	53.7 (370)	17.0	18.4 (25)	102.4 (705)	52.4 (361)	15.5	17.7 (24)
CA 4-1	4.26	5.02	8.39	1.26	0.8	84.6 (583)	39.8 (274)	37.0	54.6 (74)	91.7 (632)	46.7 (322)	13.0	17.7 (24)
CA 4-2	4.29	4.84	8.72	1.26	0.9	92.8 (639)	46.1 (318)	23.0	39.1 (53)	103.3 (712)	50.5 (348)	20.0	21.4 (29)
CA 4-3	4.22	5.13	9.23	1.26	0.8	107.7 (742)	50.9 (351)	19.0	23.6 (32)	104.6 (721)	49.2 (339)	26.0	21.4 (29)
CA 5-1	4.45	4.10	9.10	0.88	1.1	96.5 (665)	46.8 (322)	23.0	31.7 (43)	103.5 (713)	50.2 (346)	25.0	20.7 (28)
CA 5-2	4.54	4.10	9.33	0.83	1.1	111.2 (766)	55.8 (384)	20.0	17.7 (24)	105.3 (725)	53.0 (365)	22.0	19.9 (27)
CA 5-3	4.24	4.22	9.87	0.84	1.0	121.6 (838)	70.7 (487)	16.0	11.1 (15)	110.1 (759)	59.0 (407)	26.0	17.7 (24)
CA 6-1	4.44	3.08	8.83	1.26	1.4	92.4 (637)	49.6 (342)	19.0	31.7 (43)	102.0 (703)	49.0 (338)	25.0	21.4 (29)
CA 6-2	4.42	2.96	9.39	1.24	1.5	109.3 (753)	52.7 (363)	20.0	18.4 (25)	104.2 (718)	53.5 (369)	22.0	19.9 (27)
CA 6-3	4.35	2.96	9.90	1.24	1.5	123.0 (847)	69.0 (475)	15.0	12.5 (17)	108.4 (747)	52.0 (358)	28.0	17.7 (24)
CA 7-1	4.30	4.28	8.44	1.21	1.0	86.4 (595)	41.5 (286)	21.5	42.0 (57)	97.2 (670)	44.3 (305)	22.0	23.6 (32)
CA 7-2	4.11	4.39	8.78	1.23	0.9	101.2 (697)	48.7 (335)	27.5	29.5 (40)	102.5 (706)	48.6 (335)	20.0	23.6 (32)
CA 7-3	4.40	4.39	9.34	1.20	1.0	111.5 (768)	55.9 (385)	21.0	19.2 (26)	104.2 (718)	50.0 (345)	20.0	23.6 (32)

Table 2. (cont'd)

Composition, wt %						Mechanical Properties							
						Concast				Concast + 700°C 6 h. air cooled			
Sample No.	Ni	Fe	Al	Mn	Ni/Fe Ratio	UTS ksi (MPa)	0.5% YS, ksi (MPa)	El% on 2 in. (51 mm)	Charpy impact ft-lb (J)	UTS YS, (MPa)	0.5% YS, ksi (MPa)	El% on 2 in. (51 mm)	Charpy impact ft-lb (J)
CA 8-1	4.58	3.66	8.09	0.65	1.2	76.2 (525)	35.8 (247)	46.0	84.8 (115)	-	46.2 (318)	3[a]	-
CA 8-2	4.58	3.67	8.47	0.70	1.2	88.0 (606)	38.8 (267)	34.0	38.4 (52)	94.5 (651)	43.8 (302)	23.0	23.6 (32)
CA 8-3	4.60	3.68	8.77	0.70	1.2	94.6 (652)	44.3 (305)	28.0	33.2 (45)	101.3 (698)	49.8 (343)	21.0	22.1 (30)
CA 9-1	4.53	4.48	8.09	0.65	1.0	79.3 (546)	35.5 (245)	44.0	79.7 (108)	91.6 (631)	48.8 (336)	15.0	20.7 (28)
CA 9-2	4.51	4.51	8.58	0.68	1.0	90.8 (626)	40.3 (278)	29.0	37.6 (51)	97.1 (669)	46.0 (317)	24.0	25.1 (34)
CA 9-3	4.48	4.45	8.95	0.68	1.0	100.0 (689)	47.6 (328)	28.0	33.9 (46)	104.3 (719)	51.7 (356)	23.0	21.4 (29)
CA 10-1	4.42	4.89	8.09	0.68	0.9	77.7 (535)	36.5 (251)	40.0	81.9 (111)	95.2 (656)	46.7 (322)	15.0	19.9 (27)
CA 10-2	4.40	4.93	8.53	0.71	0.9	93.6 (645)	40.0 (276)	30.0	37.6 (51)	97.5 (672)	48.2 (318)	25.0	26.6 (36)
CA 10-3	4.39	4.92	8.85	0.70	0.9	102.4 (705)	45.9 (316)	31.5	31.0 (42)	103.9 (716)	51.0 (351)	24.0	21.4 (29)
CA 11-1	4.41	3.60	8.56	1.20	1.2	86.6 (597)	40.3 (278)	30.0	43.5 (59)	96.9 (668)	48.1 (331)	22.5	28.8 (39)
CA 11-2	4.40	3.44	9.10	1.19	1.3	97.4 (671)	49.3 (340)	23.0	29.5 (40)	104.5 (720)	52.8 (364)	20.5	20.7 (28)
CA 11-3	4.40	3.44	9.52	1.18	1.3	108.6 (748)	53.9 (371)	20.5	21.4 (29)	105.7 (728)	54.6 (376)	26.0	19.9 (27)
CA 12-1	4.37	4.47	8.20	1.20	1.0	84.6 (583)	38.4 (265)	36.5	58.3 (79)	96.6 (666)	46.5 (320)	21.0	25.8 (35)
CA 12-2	4.35	4.47	8.75	1.19	1.0	96.3 (663)	46.0 (317)	30.5	43.5 (59)	96.6 (666)	51.2 (353)	15.0	24.3 (33)
CA 12-3	4.37	4.52	9.09	1.18	1.0	102.5 (706)	48.8 (336)	26.0	28.8 (39)	105.3 (725)	51.3 (353)	23.0	22.1 (30)
CA 13-1	4.41	4.71	8.20	1.18	0.9	51.8[a] (357)	37.2 (256)	10.0[a]	63.4 (86)	96.8 (667)	46.4 (320)	21.0	25.1 (34)
CA 13-2	4.38	4.79	8.52	1.20	0.9	93.8 (646)	42.4 (292)	29.5	42.8 (58)	100.5 (692)	48.0 (331)	21.0	26.6 (36)
CA 13-3	4.38	4.80	9.20	1.19	0.9	102.1 (703)	47.5 (327)	29.0	32.4 (44)	105.0 (723)	51.4 (354)	23.0	22.1 (30)
CA 14-1	4.39	4.27	9.05	1.09	1.0	97.7 (673)	46.2 (318)	26.0	37.6 (51)	104.9 (723)	51.5 (355)	19.0	20.7 (28)
CA 14-2	4.39	4.90	9.05	1.07	0.9	99.4 (685)	45.8 (316)	31.0	35.4 (48)	104.8 (722)	51.5 (355)	22.5	22.1 (30)

Table 2. (cont'd)

Composition, wt %						Mechanical Properties							
						Concast				Concast + 700°C 6 h. air cooled			
Sample No.	Ni	Fe	Al	Mn	Ni/Fe Ratio	UTS ksi (MPa)	0.5% YS, ksi (MPa)	El% on 2 in. (51 mm)	Charpy impact ft-lb (J)	UTS YS, (MPa)	0.5% YS, ksi (MPa)	El% on 2 in. (51 mm)	Charpy impact ft-lb (J)
CA 14-3	4.39	5.06	8.82	1.07	0.9	100.0 (689)	45.3 (312)	32.0	34.7 (47)	102.1 (703)	47.4 (327)	25.0	21.4 (29)
Desired composition	4.5	3.5-5.0	8.25-9.25	0.8-1.30		85.0** (586)	35.0** (241)	18.0**					

*Flaw in gauge section

**Minimum mechanical properties for ASTM B505 alloy (C95800)

Table 3. Chemical compositions and mechanical properties of sand-cast and cast and heat treated keel block specimens.

Composition, wt %						Sand-cast					Sand-cast + 700°C, 6 h, air cooled				
Sample No.	Ni	Fe	Al	Mn	Ni/Fe Ratio	UTS ksi (MPa)	0.5% YS, ksi (MPa)	El% in 2 in. (51 mm)	CVN ft-lb (J)	Presence of dark etching phase	UTS ksi (MPa)	0.5% YS, ksi (MPa)	El% in 2 in. (51 mm)	CVN ft-lb (J)	Presence of dark etching phase
1950-1	4.32	4.62	8.39	0.81	0.9	85.9 (592)	31.3 (216)	23	-	NO	93.4 (643)	38.4 (265)	20.5	-	NO
1966-1	4.66	3.02	8.09	0.49	1.5	71.7 (494)	25.9 (178)	38	-	NO	83.9 (578)	46.0 (317)	15	-	NO
1973-1	4.65	5.25	8.26	0.50	0.9	92.3 (636)	34.1 (235)	32	-	NO	94.1 (648)	39.9 (275)	18	-	NO
1973-2	4.65	5.25	8.53	0.50	0.9	93.4 (643)	34.5 (238)	28.5	-	NO	95.6 (659)	44.0 (303)	17	-	NO
1997-1	4.80	4.29	9.17	0.72	1.1	82.8 (570)	33.9 (234)	21.2	-	YES	92.2 (635)	38.0 (262)	17.5	-	NO
1919-2	4.44	3.45	8.41	1.15	1.3	73.0 (503)	27.4 (189)	26	-	NO	-	38.0 (262)	-	-	NO
1941-1	4.20	4.56	8.56	1.28	0.9	87.5 (603)	31.0 (214)	31	-	NO	92.9 (640)	38.0 (262)	21	-	NO
1942-1	4.40	3.25	9.04	1.11	1.3	85.7 (590)	30.5 (210)	29.5	-	NO	93.9 (647)	41.5 (286)	22	-	NO
2042-1	4.65	4.72	8.70	0.95	1.0	87.2 (601)	30.3 (209)	36	27 (37)	NO	97.8 (674)	42.9 (296)	23	20 (27)	NO
2049-3	4.45	3.52	9.60	1.13	1.3	94.1 (648)	36.2 (249)	22	21 (28)	YES	96.0 (661)	39.0 (269)	20	21 (28)	YES
2070-1	4.61	4.78	9.20	0.58	1.0	94.7 (652)	36.4 (251)	29	31 (42)	YES	99.0 (682)	42.4 (292)	20	22 (30)	NO
2083-2	4.52	5.28	8.0	0.47	0.9	90.6 (624)	33.1 (228)	38		NO	93.4 (643)	41.5 (286)	28	33 (45)	NO
2085-1	4.76	4.79	8.75	0.77	1.0	92.5 (637)	36.9 (254)	30	40 (54)	NO	98.5 (679)	44.8 (309)	22	24 (32)	NO
2085-3	"	"	9.79	"	"	99.0 (682)	43.8 (302)	24	20 (27)	YES	97.1 (669)	45.4 (313)	19	19 (25)	YES
2086-3	4.74	3.93	8.98	0.68	1.2	91.4 (630)	33.6 (231)	29	32 (43)	YES	95.0 (655)	40.4 (278)	18	23 (31)	NO
2090-1	4.52	4.80	9.14	1.03	0.9	95.0 (655)	36.3 (250)	31	29 (39)	YES	98.6 (679)	43.3 (298)	23	20 (27)	NO
2096-3	4.70	4.36	8.10	0.93	1.1	88.4 (609)	31.3 (216)	38	54 (73)		93.4 (643)	39.9 (275)	-	29 (39)	
2100-1	4.70	4.52	8.00	0.97	1.0	87.6 (604)	32.0 (220)	39	56 (76)	NO	93.0 (641)	39.9 (275)	22	29 (39)	NO
2110-1	4.66	4.41	8.0	0.99	1.1	85.0 (586)	31.7 (218)	32	63 (85)	NO	91.5 (630)	39.2 (270)	22	31 (42)	NO

Table 3. (cont'd)

Composition, wt %						Sand-cast					Sand-cast + 700°C 6 h air cooled				
Sample No.	Ni	Fe	Al	Mn	Ni/Fe Ratio	UTS ksi (MPa)	0.5% YS, ksi (MPa)	El% in 2 in. (51 mm)	CVN ft-lb (J)	Presence of dark etching phase	UTS ksi (MPa)	0.5% YS, ksi (MPa)	El% in 2 in. (51 mm)	CVN ft-lb (J)	Presence of dark etching phase
2123-1	4.46	4.01	8.31	1.11	1.1	76.3 (526)	27.8 (191)	29	56 (76)	NO	89.2 (615)	37.8 (260)	18	32 (43)	NO
2146-1	4.76	3.58	9.0	0.82	1.3	-	-	-	38 (52)	YES	-	-	-	25 (34)	NO
2155-1	4.68	4.16	8.25	1.03	1.1	83.9 (578)	31.3 (216)	30	54 (74)	NO	93.8 (646)	40.2 (277)	21	25 (34)	NO
2166-1	4.94	4.8	8.65	0.88	1.0	89.5 (617)	34.7 (239)	31	42 (56)	NO	95.1 (655)	41.6 (287)	21	24 (32)	NO
2176-1	4.90	4.07	8.20	0.97	1.2	85.9 (592)	32.8 (226)	32	52 (70)	NO	95.2 (656)	42.0 (289)	23	26 (35)	NO
2220-1	4.47	5.0	8.60	0.87	0.9	91.2 (628)	34.0 (234)	37	44 (60)	NO	93.2 (642)	39.7 (273)	26	26 (36)	NO
2220-3	"	"	8.83	"	"	88.0 (606)	34.3 (236)	22	34 (46)	NO	92.9 (640)	37.6 (259)	19	22 (30)	NO
2243-1	4.43	5.44	8.3	1.05	0.8	89.9 (619)	35.2 (242)	29	45 (61)	NO	91.3 (629)	39.9 (275)	16	22 (30)	NO
2259-1	4.44	4.81	9.35	1.06	0.9	94.8 (653)	34.7 (239)	24	23 (31)	YES	94.8 (653)	39.2 (270)	20	20 (27)	NO
2252-1	4.47	4.33	8.40	0.86	1.0	89.2 (615)	31.3 (216)	36	54 (73)	NO	94.9 (654)	38.3 (264)	28	29 (39)	NO
2058-1	4.57	4.92	9.51	1.27	0.9	96.7 (666)	40.7 (280)	20	-	YES	95.2 (656)	41.5 (286)	16	-	NO
2024-1	4.50	4.52	8.0	0.82	1.0	86.0 (592)	29.8 (205)	36		NO	92.0 (634)	38.3 (264)	23	-	NO
2024-2	"	"	8.49	"	"	87.9 (606)	32.1 (221)	30		NO	94.6 (652)	37.8 (260)	25		NO
2024-3	"	"	9.03	"	"	91.9 (633)	33.1 (228)	28		NO	97.1 (669)	38.7 (267)	22		NO
2315-4	4.64	4.38	9.25	0.63	1.1	93.3 (643)	35.4 (244)	24		YES	94.8 (653)	39.6 (273)	16		NO

Table 5. Composition (wt %) of electrodes used in GMAW restrained butt weld tests.

	Cu	Al	Ni	Fe	Mn	Zn	Si	Density gm/mL
Ampcotrode 10	Bal	9.52	-	0.91	-	0.01	0.02	7.56
Ampcotrode 10*	Bal	9.76	-	0.87	-	0.008	0.01	
Ampcotrode 46*	Bal	9.35	4.85	4.22	1.04	-	0.02	7.59
Experimental* (in-house)	Bal	8.54	4.61	4.46	1.04	<0.005		7.68

*CANMET Wet Chemical Analysis

Table 6. Summary of welding conditions used in restrained GMAW butt welds in Ni-Al bronze alloys.

Joint design:	60° included angle single V-groove, 3/16-in. (5-mm) root gap
Electrode wire:	(a) 1/16-in. (1.6-mm) diam. Ampcotrode 10 (b) 1/16-in. (1.6-mm) diam. Ampcotrode 46 (c) 1/16-in. (1.6-mm) diam. experimental (in-house)
Torch angle:	Approx. 15° from vertical with torch pointed in direction of travel
Shielding gas:	Argon/10-15% Helium mixture, 34 cfh (1 m^3/h)
Arc voltage:	26-29 V
Current (D.C. electrode positive):	260-310 amps
Travel speed:	7-10 in./min or (3-4 mm/s)
Preheat temp.:	66°C (150°F)
Arc energy:	40-60 (kilo joules/in.) 1.6-2.4 (kilo joules/mm)
Number of passes:	9-11
Interpass temp.:	120-180°C (250-350°F)

Table 7. Tensile properties of selected alloys (as-cast, and after 6 h at 650 or 700°C).

Alloy No.	Condition	UTS, ksi(MPa)	0.5% YS ksi(MPa)	El% in 2 in. (5 mm)
CA4-1	Concast	84.6 (583)	39.8 (274)	37.0
	700°C	91.7 (632)	46.7 (322)	13.0
	650°C	94.2 (649)	49.9 (344)	12.0
CA4-2	Concast	92.8 (639)	46.1 (318)	23.0
	700°C	103.3 (712)	50.5 (348)	20.0
	650°C	106.0 (730)	55.8 (384)	21.0
CA4-3	Concast	107.7 (742)	50.9 (351)	19.0
	700°C	104.6 (721)	49.2 (339)	26.0
	650°C	106.3 (732)	55.3 (381)	15.0
CA8-3	Concast	94.6 (662)	44.3 (305)	28.0
	700°C	101.3 (698)	49.8 (343)	21.0
	650°C	104.1 (717)	55.3 (381)	19.0
CA9-1	Concast	79.3 (546)	35.5 (245)	44.0
	700°C	91.6 (631)	48.8 (336)	15.0
	650°C	95.4 (657)	50.6 (349)	13.0
CA11-1	Concast	86.6 (597)	40.3 (278)	30.0
	700°C	96.9 (668)	48.1 (331)	22.5
	650°C	107.2 (739)	58.3 (402)	19.0
CA12-1	Concast	84.6 (583)	38.4 (265)	36.5
	700°C	96.6 (666)	46.5 (320)	21.0
	650°c	97.7 (673)	50.9 (351)	18.0
CA12-2	Concast	96.3 (663)	46.0 (317)	30.5
	700°C	96.6 (666)	51.2 (353)	15.0
	650°C	106.4 (733)	58.7 (404)	20.0
CA12-3	Concast	102.5 (706)	48.8 (336)	26.0
	700°C	105.3 (725)	51.3 (353)	23.0
	650°c	107.4 (740)	58.5 (403)	21.0
CA13-3	Concast	102.1 (703)	47.5 (327)	29.0
	700°C	105.0 (723)	51.4 (354)	23.0
	650°C	106.7 (735)	58.4 (402)	22.0
CA14-3	Concast	100.0 (659)	45.3 (312)	32.0
	700°C	102.1 (703)	47.4 (327)	25.0
	650°C	104.0 (717)	52.0 (358)	21.0

Table 8. Mechanical properties of simulated sand-cast and 700°C heat-treated rod specimens† (7/8 in. or 22 mm diam)

Sample No.	Simulated sand-cast					Simulated + 700°C, 6 h, air cooled				
	UTS ksi (MPa)	0.5% YS, ksi (MPa)	El% on 2 in. (51 mm)	Charpy impact, ft-lb (J)	Presence of dark etching phase	UTS ksi (MPa)	0.5% YS, ksi (MPa)	El% on 2 in. (51 mm)	Charpy impact, ft-lb (J)	Presence of dark etching phase
CA 1-1	87.4 (602)	33.1 (228)	33.0	46.5 (63.1)	NO	91.8 (632)	36.2 (249)	26.0	30.5 (41.4)	NO
CA 1-2	90.3 (622)	34.4 (237)	26.2	29.5 (40.0)	YES	86.6 (597)	32.8 (226)	20.0	25.5 (34.6)	YES
CA 1-3	89.0 (613)	37.4 (258)	18.0	19.0 (25.8)	YES	88.8 (612)	33.2 (229)	21.5	19.0 (25.8)	YES
CA 2-1	89.5 (617)	32.5 (224)	32.7	48.0 (65.1)	NO	90.8 (626)	34.0 (234)	27.0	35.0 (47.5)	NO
CA 2-2	91.7 (632)	36.0 (248)	32.5	38.5 (52.2)	NO	92.0 (634)	34.0 (234)	33.0	31.5 (42.7)	NO
CA 2-3	92.5 (637)	36.0 (248)	34.5	33.5 (45.4)	YES/ NO	78.6* (542)	36.8 (221)	10.0*	31.5 (42.7)	NO
CA 3-1	87.5 (603)	33.3 (229)	31.7	53.0 (71.9)	NO	86.7 (597)	35.8 (247)	17.5	34.5 (46.8)	NO
CA 3-2	91.0 (627)	36.2 (249)	34.0	35.5 (48.1)	NO	92.5 (637)	34.0 (234)	31.0	31.0 (42.0)	NO
CA 3-3	90.5 (624)	33.7 (232)	24.7	28.5 (38.6)	YES	91.8 (632)	34.0 (234)	25.5	24.0 (32.5)	YES
CA 4-1	89.0 (613)	32.5 (224)	35.5	48.0 (65.1)	NO	91.4 (630)	33.8 (233)	19.0	33.0 (44.7)	NO
CA 4-2	91.0 (627)	32.5 (224)	32.2	41.0 (55.6)	NO	92.4 (637)	36.0 (248)	30.5	30.0 (40.7)	NO
CA 4-3	92.4 (637)	33.5 (231)	32.7	32.5 (44.1)	YES	93.4 (644)	37.8 (260)	30.0	29.5 (40.0)	NO
CA 5-1	91.4 (630)	31.2 (215)	35.0	35.0 (47.5)	NO	92.3 (636)	36.2 (249)	31.0	29.0 (39.3)	NO
CA 5-2	91.0 (627)	32.3 (222)	24.5	26.0 (35.3)	YES	92.7 (639)	37.6 (259)	27.5	26.0 (35.3)	YES
CA 5-3	95.8 (660)	36.3 (250)	20.5	18.0 (24.4)	YES	94.6 (652)	38.8 (267)	24.0	20.0 (27.1)	YES
CA 6-1	89.9 (619)	34.0 (234)	35.0	30.0 (40.7)	YES	91.4 (630)	36.8 (254)	30.0	27.5 (37.3)	NO
CA 6-2	89.2 (615)	34.0 (234)	24.0	20.0 (27.1)	YES	90.9 (626)	40.0 (276)	22.5	22.0 (29.8)	YES
CA 6-3	91.6 (631)	35.1 (242)	17.5	16.0 (21.7)	YES	93.5 (644)	38.8 (267)	21.0	18.5 (25.1)	YES
CA 7-1	85.8 (591)	30.5 (210)	31.2	46.5 (63.1)	NO	91.8 (632)	39.6 (273)	25.0	30.0 (40.7)	NO
CA 7-2	90.7 (625)	32.0 (220)	40.0	36.5 (49.5)	YES/ NO	93.6 (645)	38.4 (265)	33.0	28.0 (38.0)	NO
CA 7-3	89.2 (615)	35.7 (246)	23.0	27.0 (36.6)	YES	93.2 (642)	37.0 (255)	26.5	24.0 (32.5)	YES

†See Table 2 for chemical compositions

Table 8. (cont'd)

Sample No.	Simulated sand-cast					Simulated + 700°C, 6 h, air cooled				
	UTS, ksi (MPa)	0.5% YS, ksi (MPa)	El% on 2 in. (51 mm)	Charpy impact, ft-lb (J)	Presence of dark etching phase	UTS ksi (MPa)	0.5% YS, ksi (MPa)	El% on 2 in. (51 mm)	Charpy impact, ft-lb (J)	Presence of dark etching phase
CA 8-1	88.1 (607)	32.8 (226)	33.5	43.0 (58.3)	NO	88.7 (611)	35.6 (245)	28.0	41.0 (55.6)	NO
CA 8-2	87.0 (599)	34.1 (235)	29.5	37.0 (50.2)	NO	87.0 (599)	31.6 (218)	27.0	32.0 (43.4)	NO
CA 8-3	88.8 (612)	37.3 (257)	28.0	31.0 (42.0)	YES	91.8 (632)	33.4 (230)	33.0	29.0 (39.3)	NO
CA 9-1	91.0 (627)	34.7 (239)	31.2	48.5 (65.8)	NO	90.9 (626)	34.9 (240)	28.5	40.0 (54.2)	NO
CA 9-2	90.6 (624)	34.0 (234)	28.5	38.0 (51.5)	NO	90.0 (620)	33.0 (227)	27.0	33.0 (44.7)	NO
CA 9-3	93.5 (644)	34.7 (239)	29.2	34.0 (46.1)	YES	93.5 (644)	34.0 (234)	34.5	31.0 (42.0)	NO
CA 10-1	92.3 (636)	34.8 (240)	29.0	45.0 (61.0)	NO	92.2 (635)	37.6 (259)	27.0	33.0 (44.7)	NO
CA 10-2	93.2 (642)	33.9 (234)	29.7	38.5 (52.2)	NO	92.8 (639)	34.9 (240)	28.0	32.0 (43.4)	NO
CA 10-3	95.1 (655)	34.3 (236)	33.5	34.0 (46.1)	YES	93.9 (647)	34.4 (237)	32.0	30.0 (40.7)	NO
CA 11-1	88.4 (609)	33.3 (229)	32.2	32.0 (43.4)	NO	81.1 (559)	33.8 (233)	28.5	33.0 (44.7)	NO
CA 11-2	93.3 (643)	35.0 (241)	32.2	28.5 (38.6)	YES	93.0 (641)	34.8 (240)	29.0	26.0 (35.3)	NO
CA 11-3	89.9 (619)	35.8 (237)	21.0	26.0 (35.3)	YES	91.0 (627)	34.1 (235)	21.5	25.0 (33.9)	YES
CA 12-1	89.8 (619)	32.9 (227)	32.0	45.5 (61.7)	NO	90.0 (620)	34.7 (239)	29.5	35.0 (47.5)	NO
CA 12-2	92.8 (639)	34.2 (236)	31.5	36.0 (48.8)	NO	93.1 (641)	33.5 (231)	35.0	34.0 (46.1)	NO
CA 12-3	94.3 (650)	34.9 (240)	32.5	32.5 (44.1)	YES	94.2 (649)	33.5 (231)	36.5	29.0 (39.3)	NO
CA 13-1	90.6 (624)	32.4 (223)	31.7	44.5 (60.3)	NO	91.0 (627)	35.1 (242)	28.0	33.0 (44.7)	NO
CA 13-2	92.9 (640)	33.4 (230)	31.7	39.0 (52.9)	NO	92.2 (635)	33.5 (231)	27.5	33..0 (44.7)	NO
CA 13-3	94.8 (653)	35.6 (245)	34.7	33.0 (44.7)	YES	94.2 (649)	35.0 (241)	34.5	30.0 (40.7)	NO
CA 14-1	93.8 (646)	34.3 (236)	32.2	32.0 (43.4)	YES	93.4 (643)	36.2 (249)	32.5	31.0 (42.0)	NO
CA 14-2	94.5 (651)	36.6 (252)	34.5	35.5 (48.1)	YES	93.3 (643)	36.5 (251)	35.5	30.0 (40.7)	NO
CA 14-3	94.0 (648)	37.9 (261)	36.0	35.0 (47.5)	YES	93.8 (646)	38.0 (262)	30.0	28.0 (38.0)	NO
	85.0**	35** (241)	15.0**							

**Minimum mechanical properties of ASTM B148 (Alloy C958000)

Table 9. Presence of the dark etching phase (γ_2) in simulated and sand cast alloys.

As-cast	Cast + 700°C, 6 h
Present for Al > 8.8% for Mn > 0.7%	(i) removed for 8.8 < Al < 9.0% if Mn < 1.2% (ii) removed for 9.0 < Al < 9.25% if Mn < 1.0% (iii) not removed for Al > 9.25% if Mn > 0.8%

Table 10. Chemical analysis (wt %) of phases present in sand cast and cast and 700°C heat treated NAB alloy (thin foil electron microscopy)

Phase / specimen condition	Present Work					Culpan and Rose (21)					Lloyd et al (20)					Thomson and Dion† (24)			
	Cu	Ni	Fe	Al	Mn	Cu	Ni	Fe	Al	Mn	Cu	Ni	Fe	Al	Mn	Cu	Ni	Fe	Al
α, as cast	71.4	4.7	2.3	20.5	1.1	86±4	3±2	2.4±1	8±2	0.8±0.3	82	3.5	3.6	10.9	1.2				
κ_I, as cast						15±5*	15±3*	55±7*	13±5*	2±0.4*	14**	2.8**	67**	10.5**	2.9**	10.8^1	-	78.6^1	10.6^1
																10.8^2	27.7^2	43.6^2	18^2
κ_{II}, as cast	26.9	21.3	24.1	26.0	1.7	23±4	24±5	34±5	18±4	1.6±0.3	18**	9.2**	52**	15.3**	2.5**				
κ_{III}, as cast	30.6	20.7	18.5	28.3	1.9	26±4	28±5	22±5	22±4	1.6±0.4	27.7	30.5	15	24	1.9	16^3	36.3^3	-	27.3^3
κ_{IV}, as cast	30	4	51	13	2	23±6	6±4	60±8	9±4	1.6±0.4	15.6	8.2	57.5	14.1	2				
Round ppt cast +700°C	26.7	13.2	37.6	21	1.5														
small platelet ppt cast +700°C	30.2	22.3	17.2	29.1	1.2														

*From SEM

**From extraction replica

†Wet chemical analysis of extracted phases

[1]Ternary alloy containing 8.84% Al and 3.11% Fe

[2]Complex aluminum bronze containing 8.63% Al, 4.03% Ni, 4.83% Fe

[3]Ternary alloy containing 8.62% Al and 7.4% Ni

Table 11. Transverse tensile and impact properties of GMA welds in NAB alloys

Weld No.	As Welded				Welded +700°C, 6h, Air Cooled			
	UTS ksi (MPa)	0.5% YS, ksi (MPa)	% Elong. in 2 in. (51 mm)	CVN impact energy ft-lb (J)	UTS ksi (MPa)	0.5% YS, ksi (MPa)	% Elong. in 2 in. (51 mm)	CVN impact energy ft-lb (J)
2057-2	96.5 (665)	46.1 (318)	13	16 (22)	100.5 (692)	45.2 (311)	16	16 (22)
2064	83.0 (572)	38.5 (265)	18	38 (51)	94.6 (652)	44.1 (304)	15	22 (30)
2072	96.0 (661)	48.5 (334)	12	29 (39)	102.5 (706)	47.5 (327)	17	20 (27)
2087-1	96.3 (663)	45.1 (311)	16	-	-	-	-	- -
2110-2	92.5 (637)	40.0 (278)	28	38 (51)	99.0 (682)	48.0 (331)	16	23 (31)
2111-2	*	41.5 (286)	*	35 (47)	*	49.6 (342)	*	21 (28)
2111-3++	*	37.8 (260)	*	-	*	39.4 (271)	*	-
2140-2	78.7 (542)	37.4 (258)	15	35 (48)	92.1 (635)	43.4 (299)	15	24 (32)
2141-3	80.5 (555)	38.0 (262)	12	37 (50)	92.5 (637)	45.0 (310)	13	21 (29)
2148-1++	*	40.4 (278)	*	-	*	38.9 (268)	*	-
2150-1	92.6 (638)	41.8 (288)	27	36 (49)	99.8 (688)	48.6 (335)	18	23 (31)
2150-2+	*	38.7 (267)	*	57 (78)	*	37.7 (260)	*	76 (103)
2153-1	86.8 (598)	43.5 (300)	14.5*	35 (48)	95.8 (660)*	51.4 (354)	10*	21 (28)
2156-2**	*	49.3 (340)	*	31 (42)	*	44.6 (307)	*	21 (28)
2166-2	*	43.9 (302)	*	-	-	-	-	- -
2184-2	97.7 (673)	46.9 (323)	17	30 (41)	98.0 (675)	43.3 (298)	15	21 (29)
2236-1+++	81.8 (564)	35.8 (247)	17	41 (56)	92.5 (637)	44.1 (304)	13	27 (36)

*Flaw (oxidized defect) in gauge section. All these fractures occured in the fusion zone. All other fractures occured in the parent metal.

**The plates were heat treated at 700C for 6 h and then air cooled prior to MIG welding.

+ Ampcotrode 10 filler wire

++ Ampcotrode 10 and 46 filler wires

+++ New low aluminum filler wire

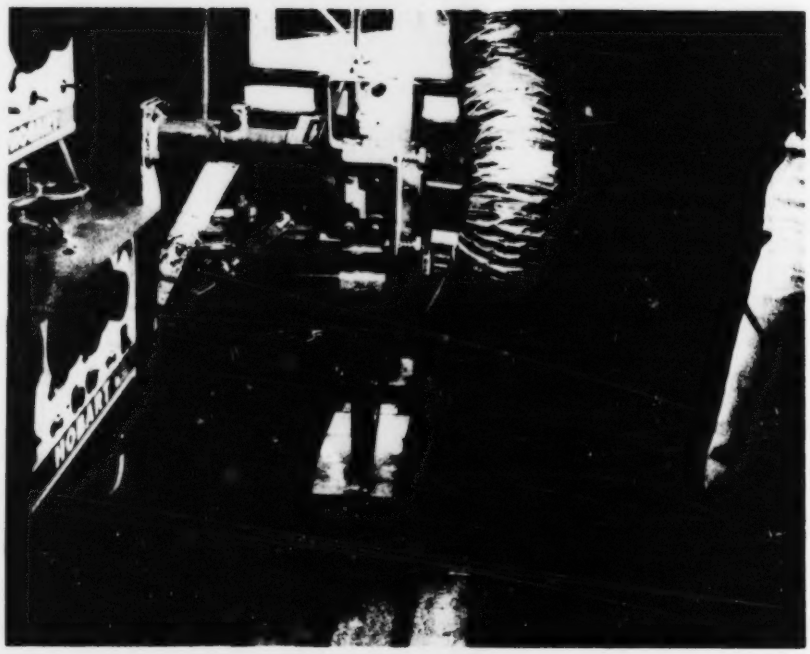

Fig. 1. Welding jig used for restrained GMAW tests. (neg 5604)

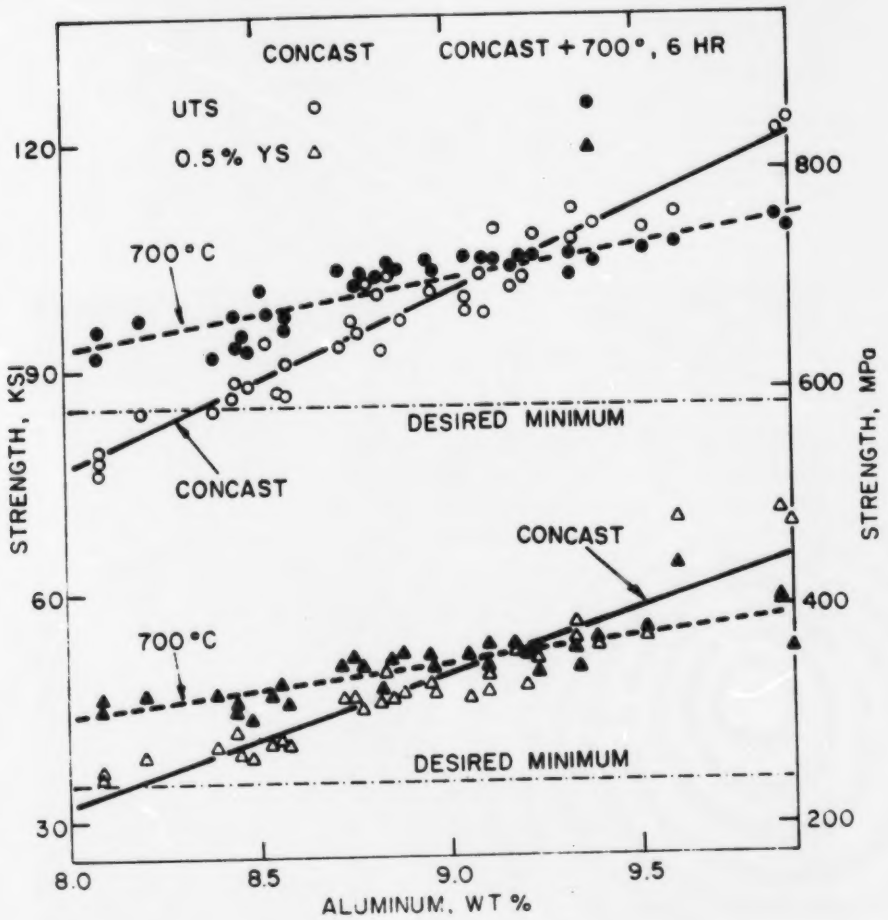

Fig. 2. Showing 0.5% yield and ultimate tensile strengths of all alloys listed in Table 2. Solid lines are for as-cast materials, and dashed lines the values after heat treatment at 700°C for 6 h. The "desired minimum" refers to 85 ksi (586 MPa) ultimate and 35 ksi (240 MPa) yield strengths in ASTM B505 (alloy C95800). (neg 1321)

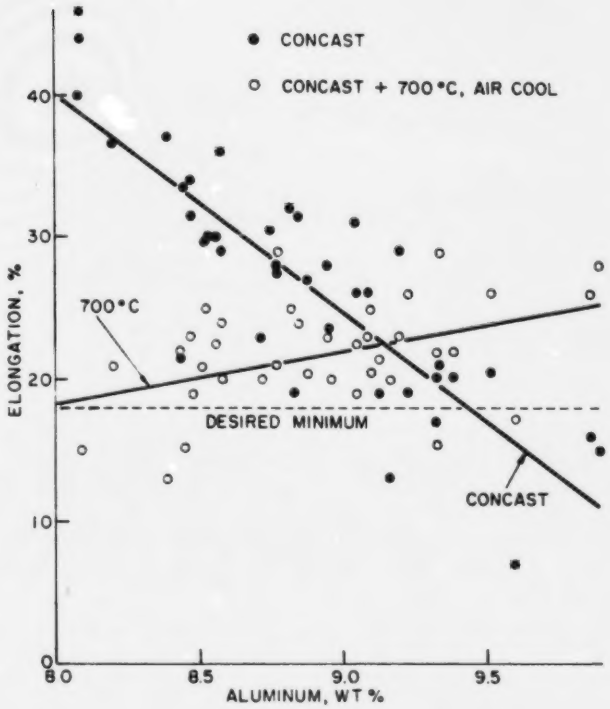

Fig. 3. Tensile elongation data from 2 in. (51 mm) gauge lengths for all alloys listed in Table 2 in both as-cast and cast-and heat-treated conditions (700 C, 6 h). Desired minimum elongation for C95800 in ASTM B505 is as shown at 18%. (neg 1324)

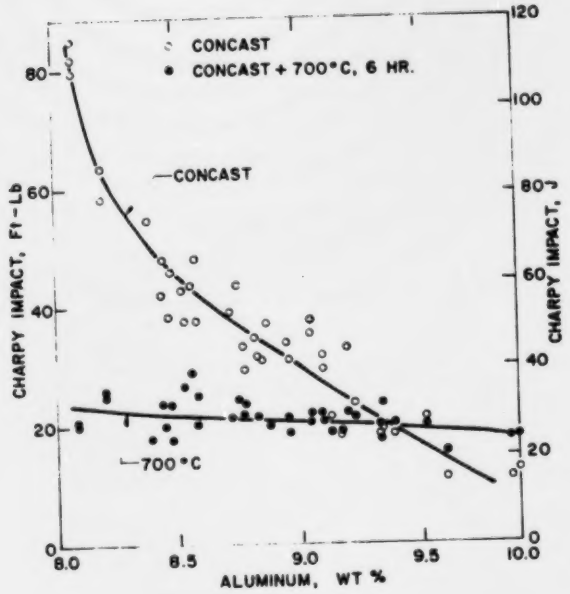

Fig. 4. Room temperature Charpy V-notch impact data for all alloys in Table 2 in both the cast, and cast and heat-treated conditions (700°C, 6 h). (neg 1344)

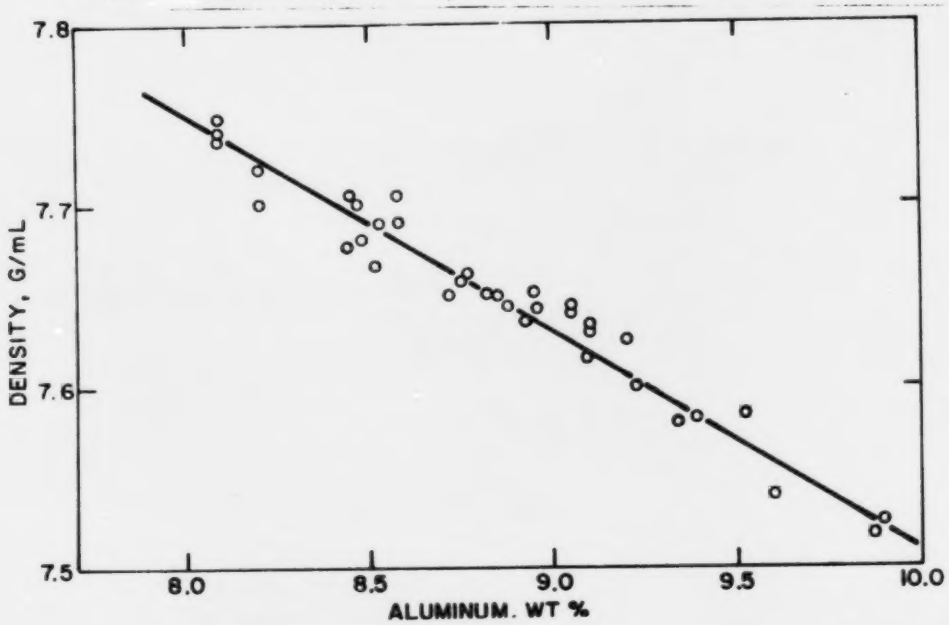

Fig. 5. Density data on continuously cast nickel-aluminum bronze alloys as a function of aluminum content, for all compositions listed in Table 2. (neg 1322)

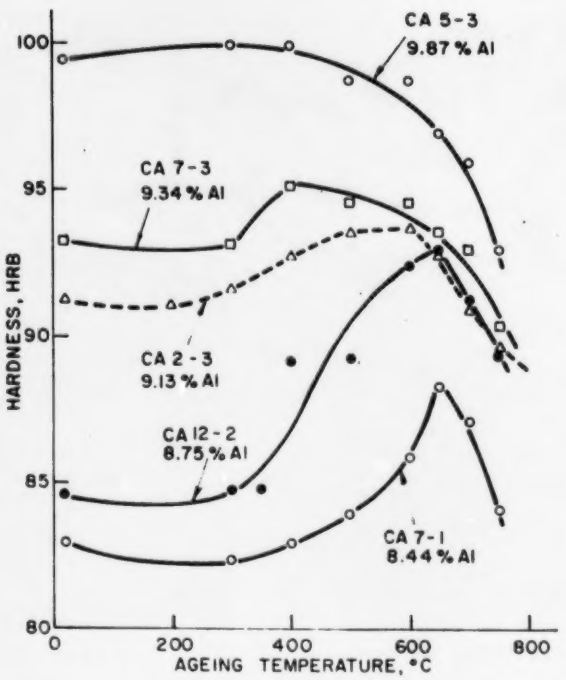

Fig. 6. Rockwell B hardness at room temperature of selected compositions (see Table 2), continuously cast and then heat-treated for 3 h at the indicated temperatures. Specimens were air-cooled from precipitation aging treatments. (neg 1330)

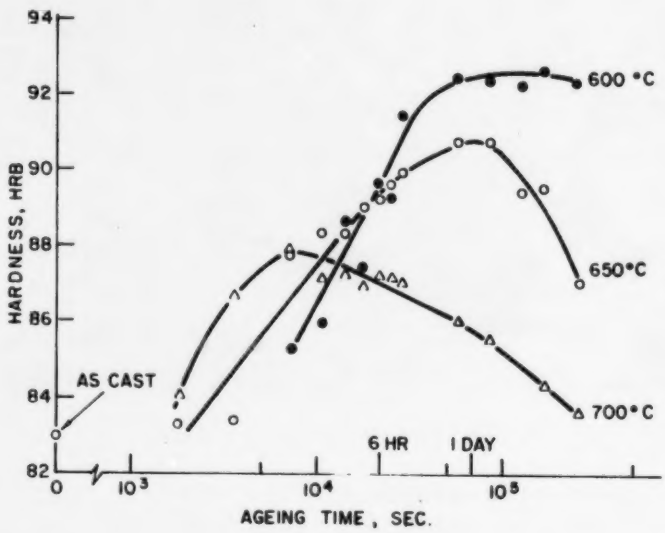

Fig. 7. Rockwell B hardness values at room temperatures vs. time at 600°C and 700°C for concast CA7-1 (8.44 Al, 4.30 Ni, 4.28 Fe and 1.21 Mn). (neg 1326)

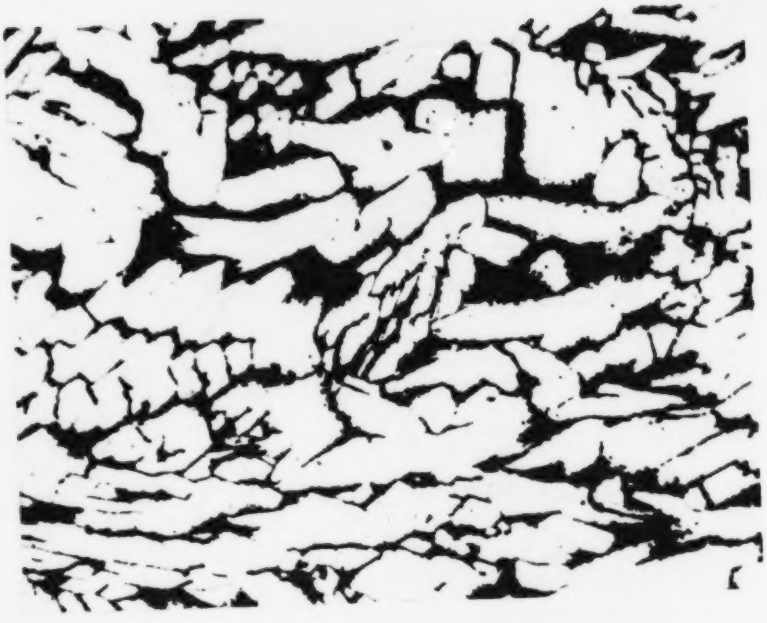

(a) alloy CA7-1, 8.5% Al. (neg 7516)

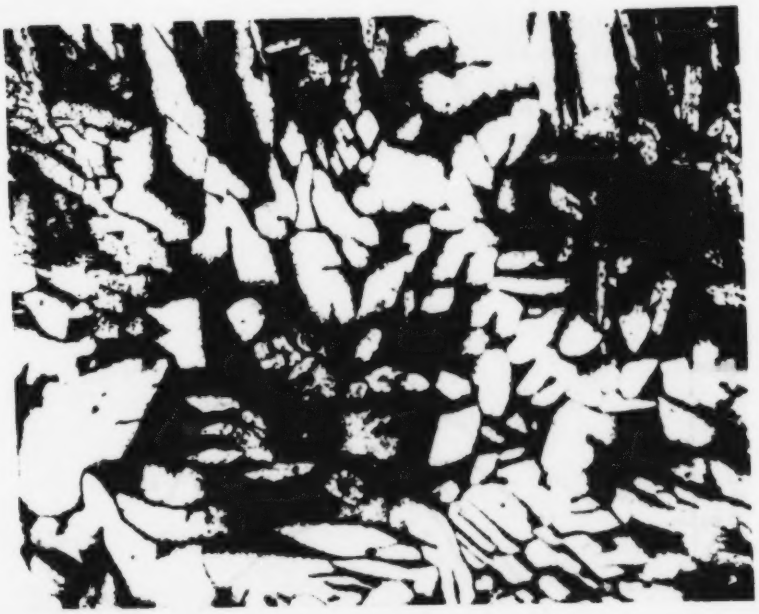

(b) alloy CA7-3, 9.3% Al. (neg 7515)

Fig. 8. Optical photomicrographs of the concast structures. Alcoholic ferric chloride etch. X1000.

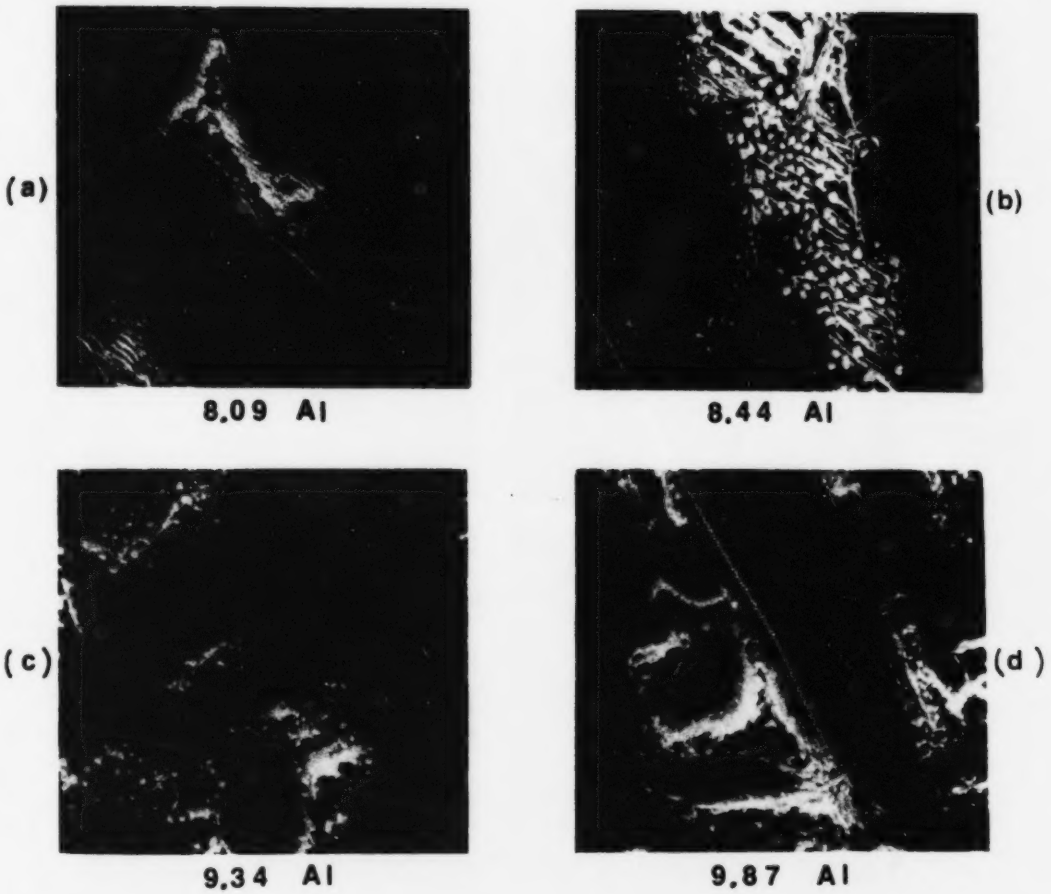

Fig. 9. SEM photomicrographs of secondary phases in four continuously cast compositions having Ni:Fe = 1. (a) CA 9-1; (b) CA 7-1; (c) CA7-3; (d) CA 5-3. The dark etching phase in $\alpha + \kappa$ eutectoid areas is $\alpha + \gamma_2$. Alcoholic ferric chloride etch. X5000. (neg 1312)

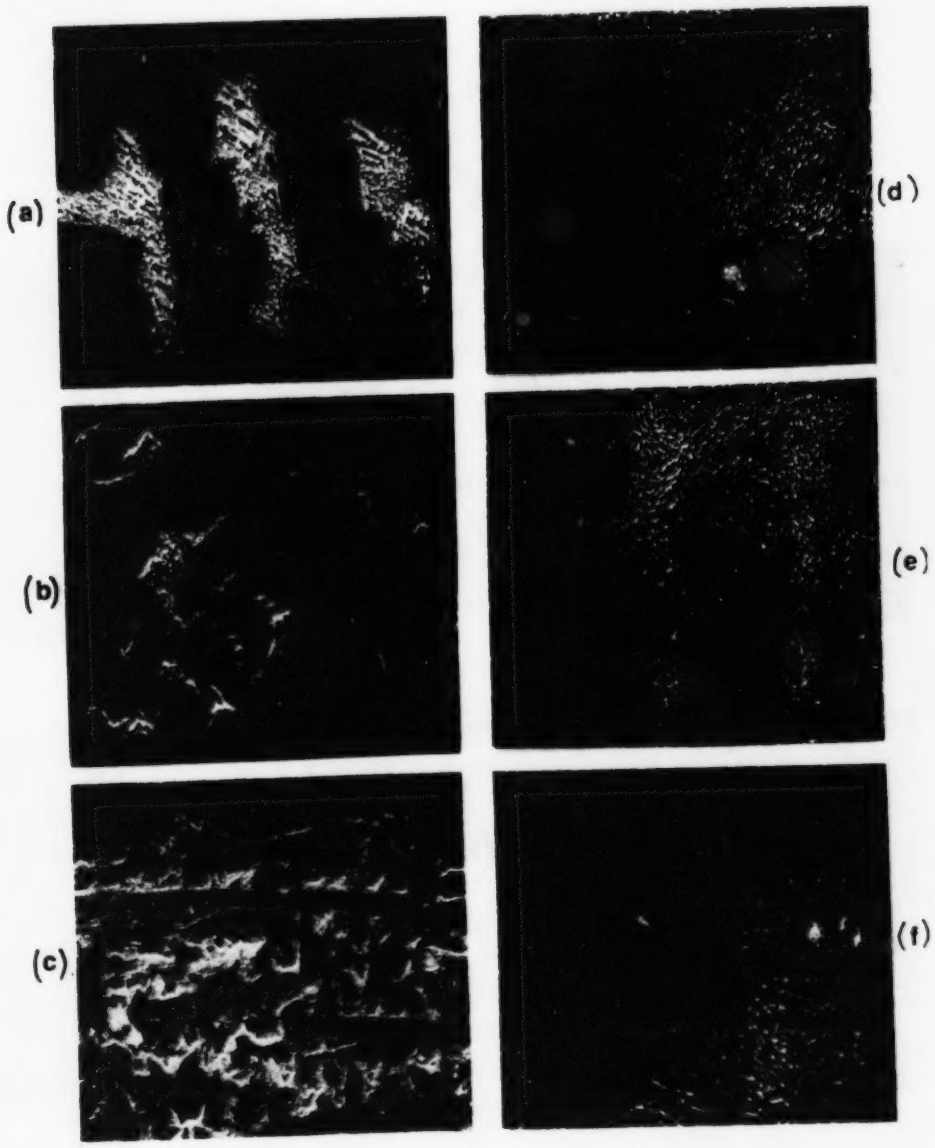

Fig. 10. SEM photomicrographs comparing cast and heat-treated materials. (a) CA 7-1, as-cast; (b) CA 7-3, as-cast; (c) CA 5-3, as-cast;(d) CA 7-1, after 700°C for 6 h; (e) CA 7-3, after 700°C for 6 h; (f) CA 5-3, after 700°C for 6 h. The heat treatment has eliminated $\alpha + \gamma_2$, coarsened the κ constituent of eutectoid, and precipitated large numbers of fine κ phase particles in the α matrix. Alcoholic ferric chloride etch. X2000. (neg 1311)

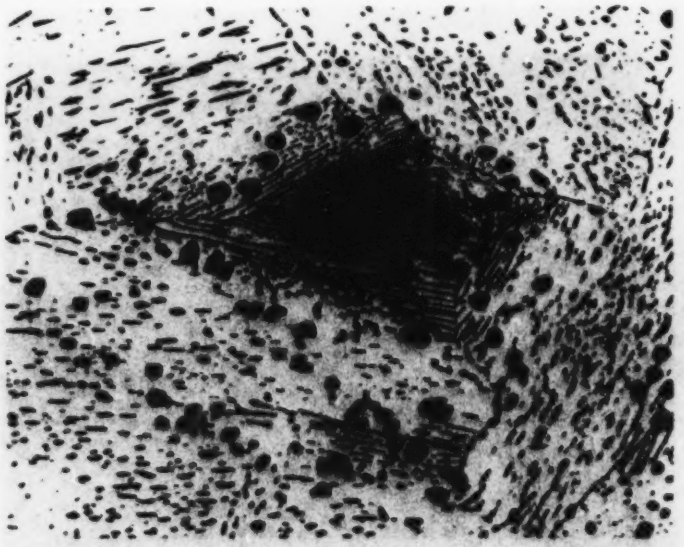

SIMULATED, X1000

(CA9-3)

8.95% AL. 4.48% NI,

4.45% FE, 0.68% MN,

NI:FE = 1.01

SAND-CAST, X1000

(2024-4)

9.01% AL, 4.36% NI,

4.41% FE, 0.86% MN,

NI:FE = 0.99

Fig. 11. Microstructures showing dark etching $\alpha + \gamma_2$ eutectoid at centre of nickel-rich lamellar K areas. Note precipitate in α matrix. (neg 1271)

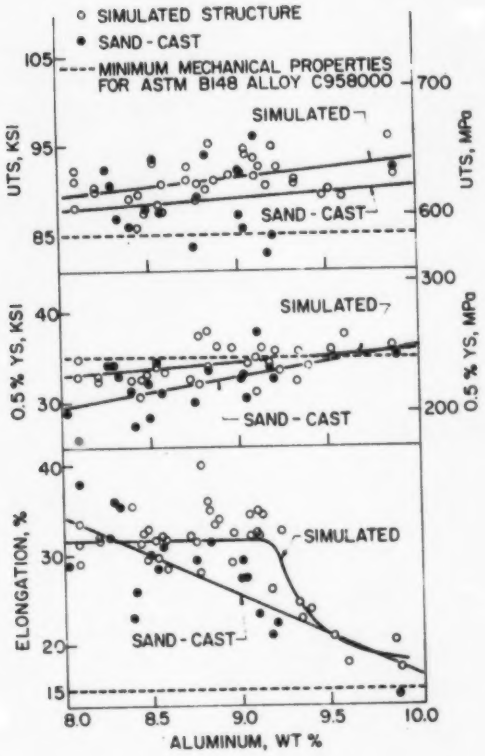

Fig. 12. Mechanical properties of simulated and sand-cast materials. (neg 1331)

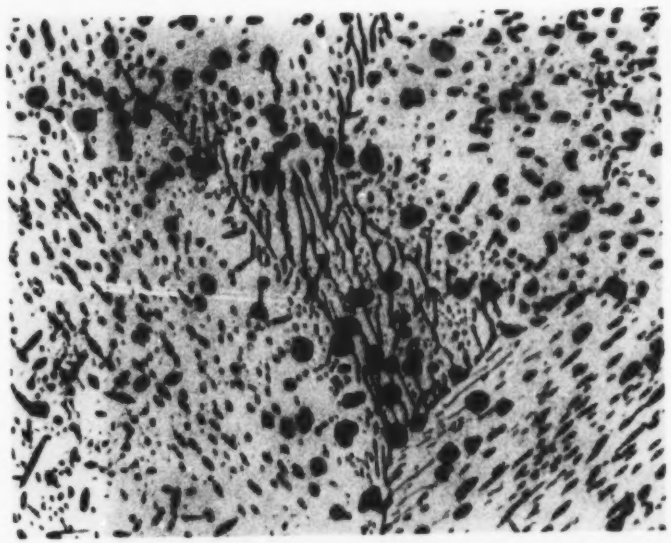

SIMULATED , X1000

(CA9-3)

8.95% AL, 4.48% NI,

4.45% FE, 0.68% MN,

NI:FE = 1.01

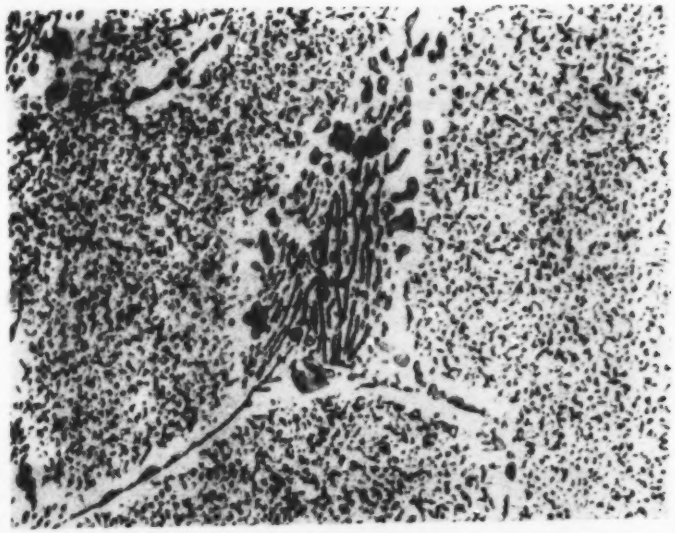

SAND-CAST , X1000

(2024-4)

9.01% AL, 4.36% NI,

4.41% FE, 0.82% MN

NI:FE = 0.99

Fig. 13. Microstructures of material after corrosion inhibiting heat treatment of 6 h at 700°C followed by air cooling. Compared with Fig. 11, note disappearance of $\alpha + \gamma_2$ eutectoid, and marked precipitation in α phase of sand-cast microstructure. (neg 1270)

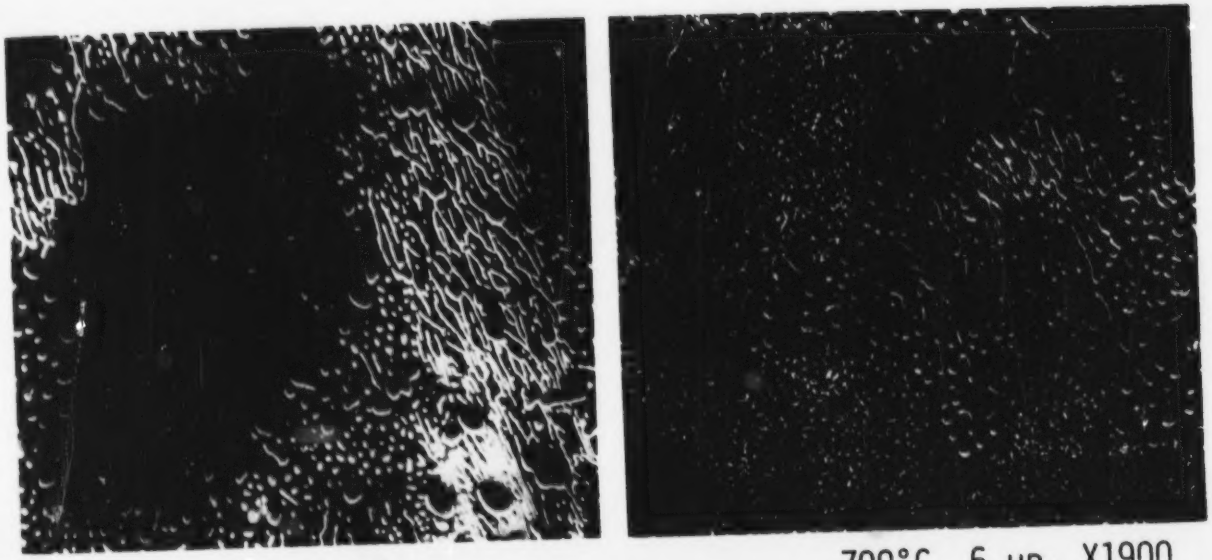

SAND-CAST, X2100

700°C, 6 HR, X1900

#2023-2, 8.81% AL, 4.53% NI

3.34% FE, 0.96% MN, NI:FE = 1.36

Fig. 14. SEM micrograph of sand-cast material before and after 6 h at 700°C treatment. (neg 1266)

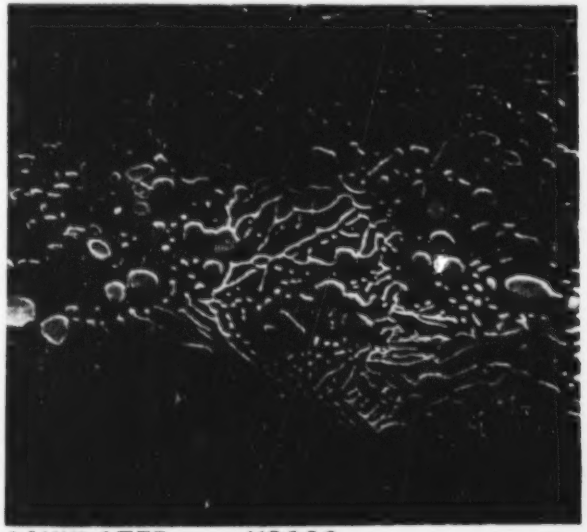

SIMULATED X2100

700°C, 6 HR, X2000

CA 12-2, 8.75%AL, 4.35% NI

4.47% FE, 1.19% MN, NI:FE = 0.97

Fig. 15. SEM micrograph of simulated material before and after 6 h at 700°C heat treatment. (neg 1267)

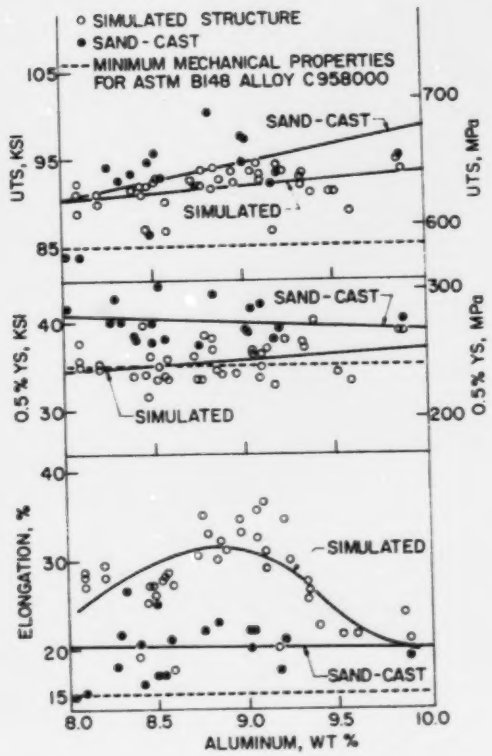

Fig. 16. Mechanical properties of simulated and sand-cast materials after 6 h at 700°C heat treatment. (neg 1315)

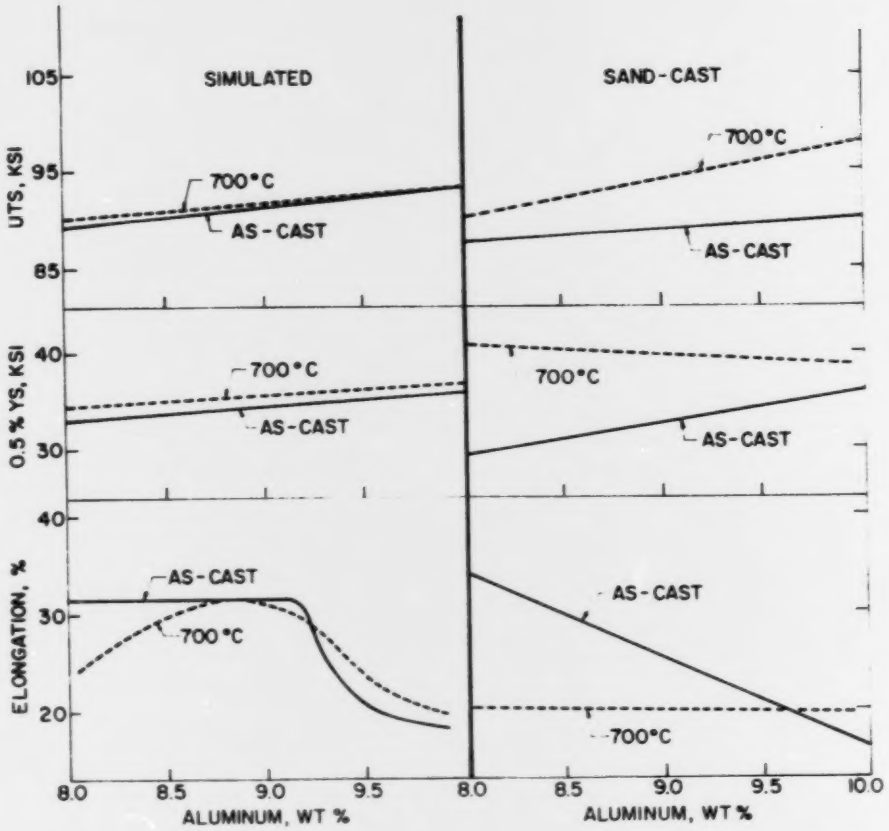

Fig. 17. Comparison of mechanical properties of simulated and sand-cast materials before and after 6 h at 700°C heat treatments. (neg 1317)

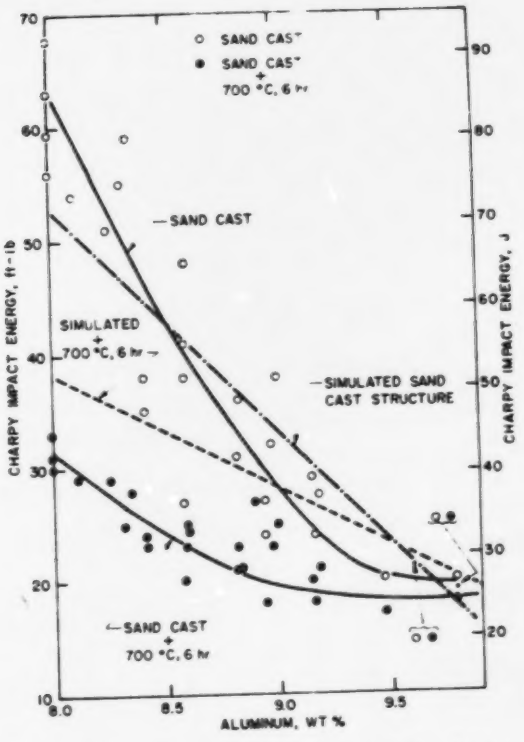
SAND CAST
SAND CAST + 700 °C, 6 hr
SAND CAST
SIMULATED + 700 °C, 6 hr
SIMULATED SAND CAST STRUCTURE
SAND CAST + 700 °C, 6 hr
CHARPY IMPACT ENERGY, ft-lb
CHARPY IMPACT ENERGY, J
ALUMINUM, WT %

Fig. 18. Room temperature Charpy V-notch impact data for simulated sand-cast, and sand-cast alloys before and after the corrosion-inhibiting heat treatment of 6 h at 700°C. (neg 2681)

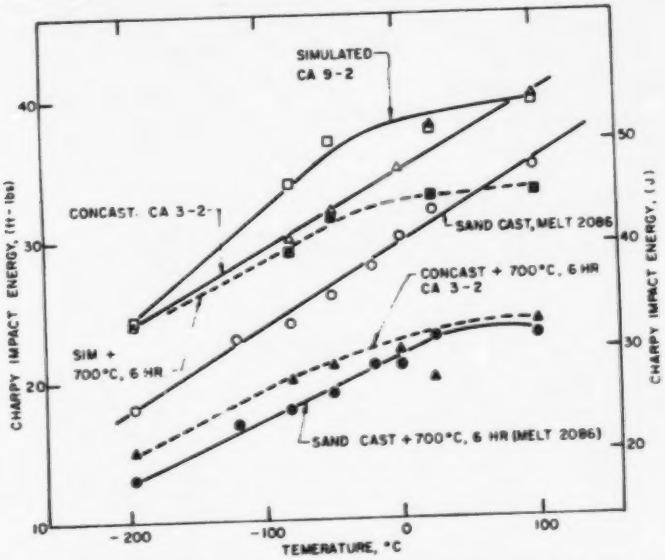
SIMULATED CA 9-2
CONCAST CA 3-2
SAND CAST, MELT 2086
CONCAST + 700°C, 6 HR CA 3-2
SIM + 700°C, 6 HR
SAND CAST + 700°C, 6 HR (MELT 2086)
CHARPY IMPACT ENERGY, (ft-lbs)
CHARPY IMPACT ENERGY, (J)
TEMERATURE, °C

Fig. 19. Charpy V-notch impact energy-temperature curves for concast (CA 3-2, 8.88% Al, 4.3% Ni, 4.58% Fe, 0.68% Mn); and sand-cast (melt No. 2086, 8.98% Al, 4.74% Ni, 3.93% Fe, 0.68% Mn) before and after the 700°C, 6 h heat treatment. (neg 2250)

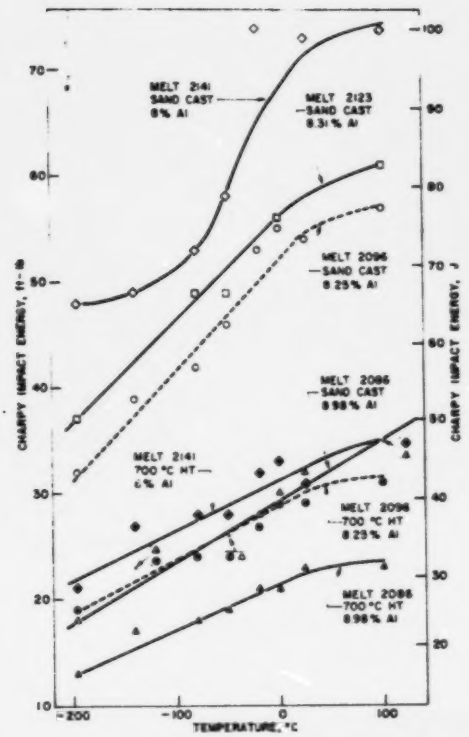

Fig. 20. Charpy V-notch impact energy-temperature plots for NAB alloys of different aluminum contents in both sand-cast, and sand-cast and 700°C heat-treated conditions. (neg 2680)

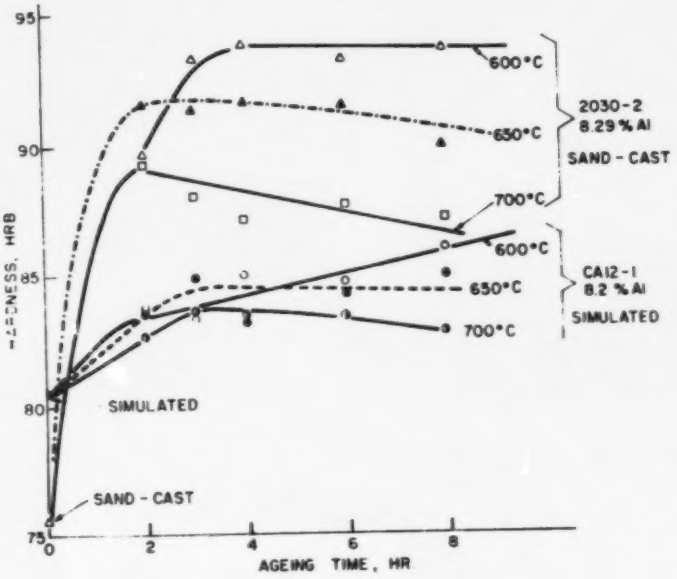

Fig. 21. Hardness response at different times and temperatures of simulated and sand-cast material. (neg 1332)

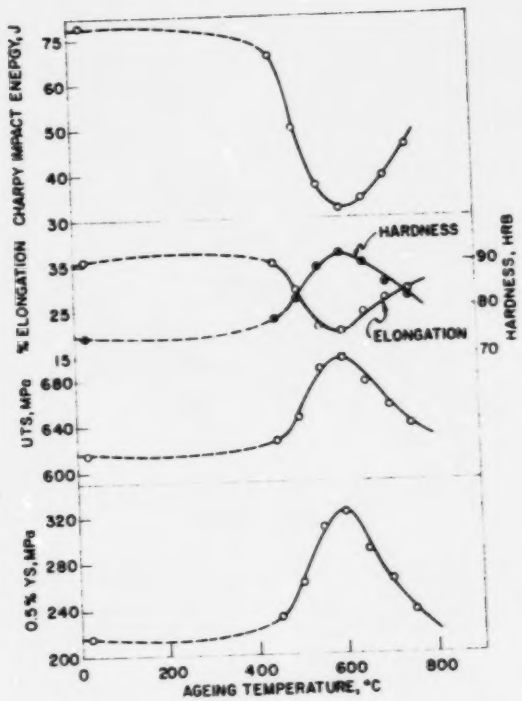

Fig. 22. Mechanical properties of sand-cast alloy #2252 (8.65% Al, 4.47% Ni, 4.33% Fe and 0.86% Mn) as a function of aging temperature. Specimens were air-cooled after the 6 h heat treatment. (neg 6984)

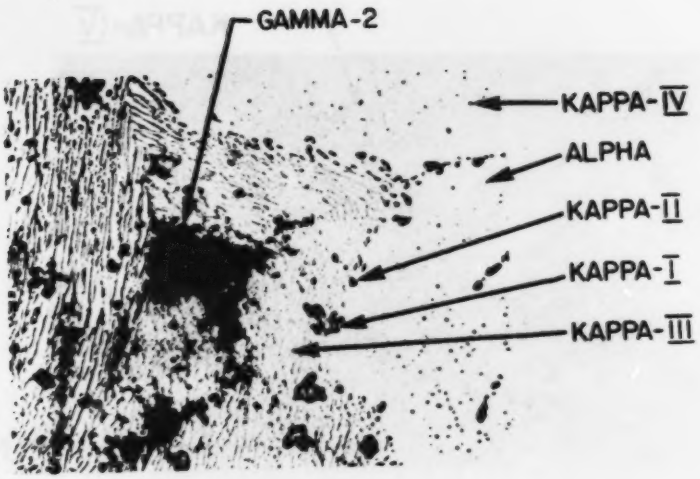

Fig. 23. Optical micrograph of sand-cast alloy 2086-3 (8.98% Al, 4.74% Ni, 3.93% Fe, 0.68% Mn) showing the various phases. Alcoholic ferric chloride etch. X650. (neg 2901)

Fig. 24. Transmission electron micrograph of sand-cast alloy 2086-3 (8.98% Al, 4.74% Ni, 3.93% Fe, 0.68% Mn) showing lamellar κ_{III} phase. X34,000. (neg 2433)

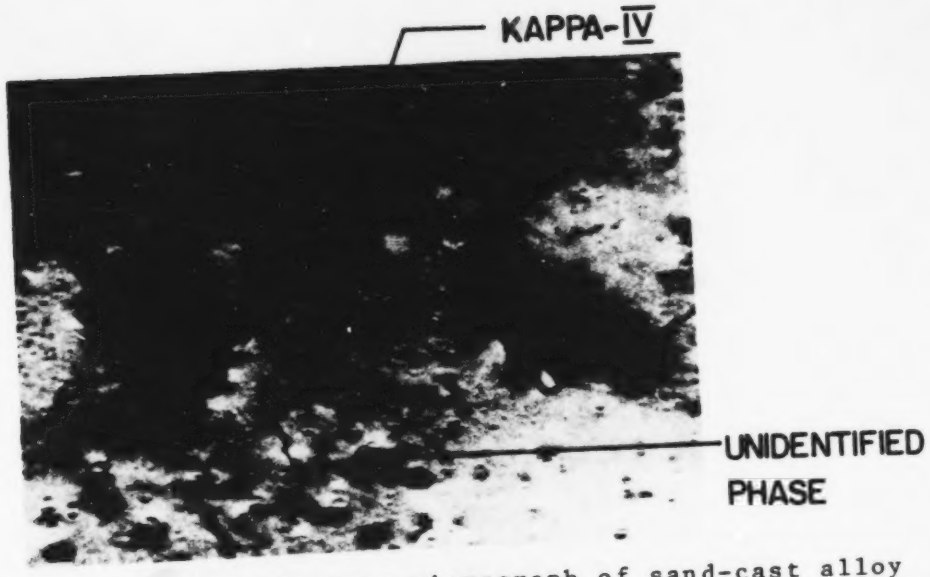

Fig. 25. Transmission electron micrograph of sand-cast alloy 2086-3 (8.98% Al, 4.74% Ni, 3.93% Fe, 0.68% Mn) showing κ_{IV} phase and unidentified phase. X34,000. (neg 2432)

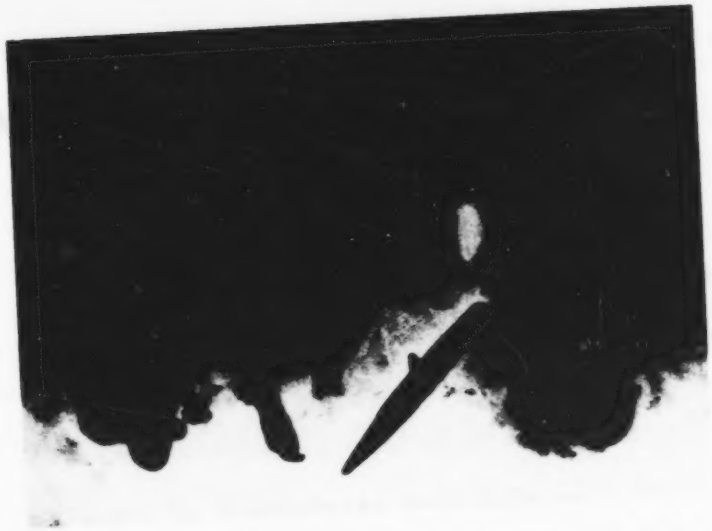

Fig. 26. Transmission electron micrograph of alloy 2086-3 (8.98% Al, 4.74% Ni, 3.93% Fe, 0.68% Mn), heat-treated at 700°C for 6 h, showing platelets and spherical precipitates in α grain. X25,000. (neg 2902)

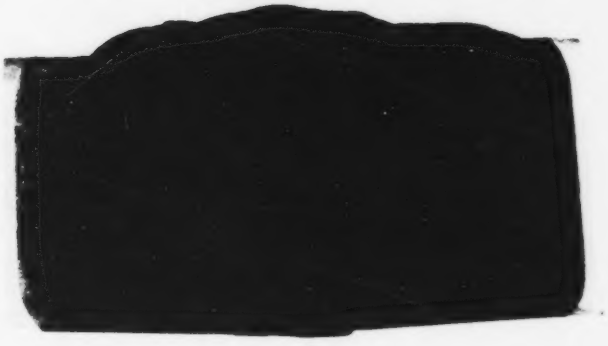

Fig. 27. Transverse section of GMAW weld 2057-2. Alcoholic ferric chloride etch. X1.5 (neg 2137)

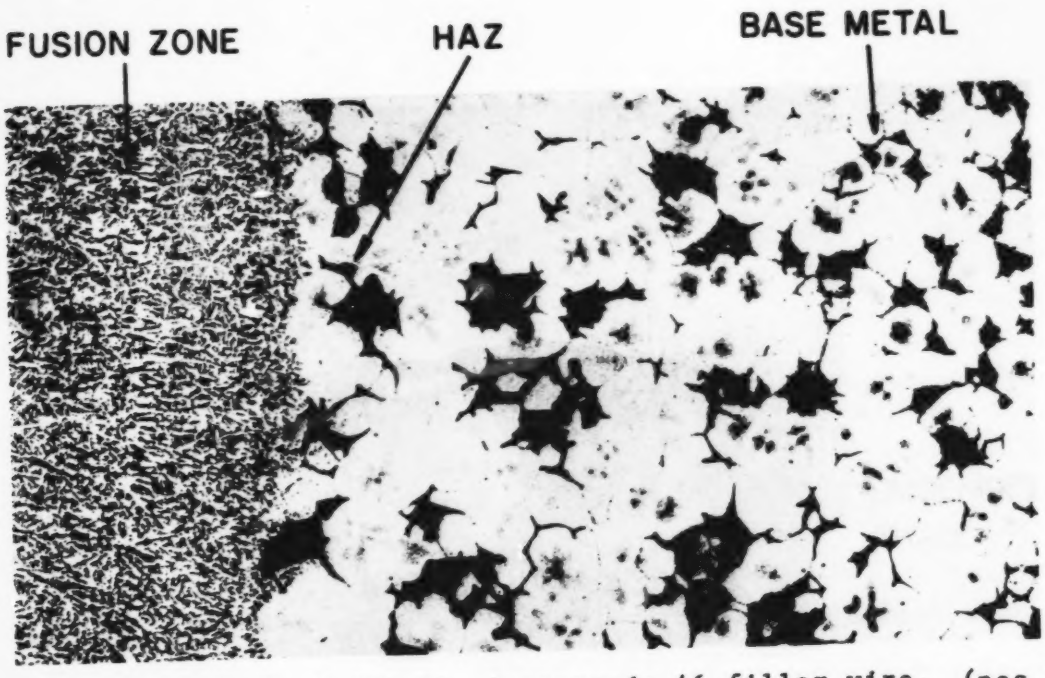

(a) weld 2111-2, 8.25% Al, Ampcotrode 46 filler wire. (neg 3292)

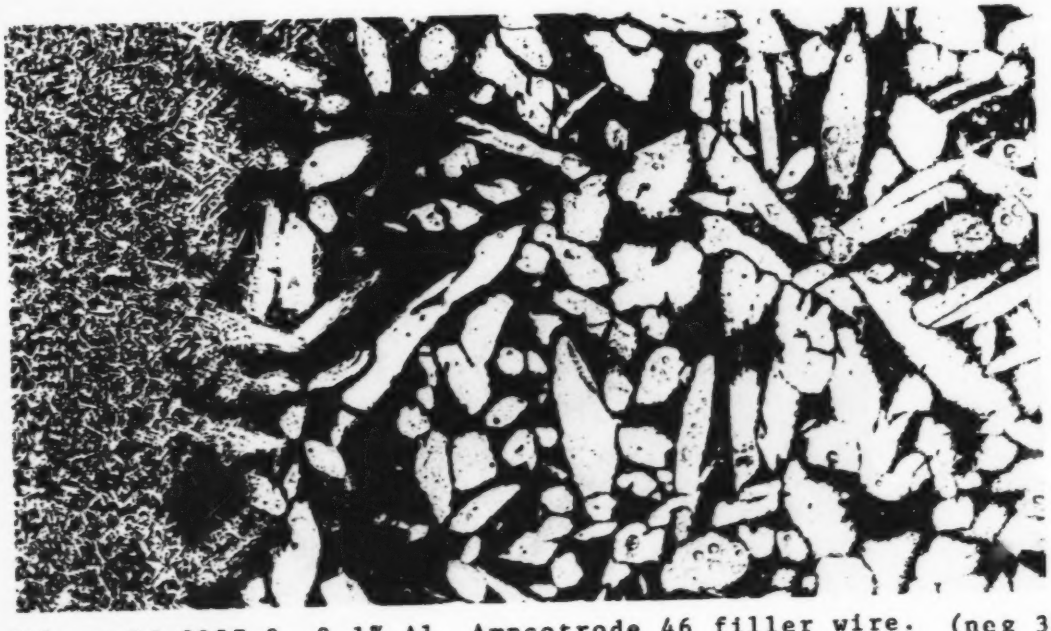

(b) weld 2057-2, 9.1% Al, Ampcotrode 46 filler wire. (neg 3290)

Fig. 28. Optical micrographs of weldments at various aluminum contents and for different filler wires. Alcoholic ferric chloride etch. X100.

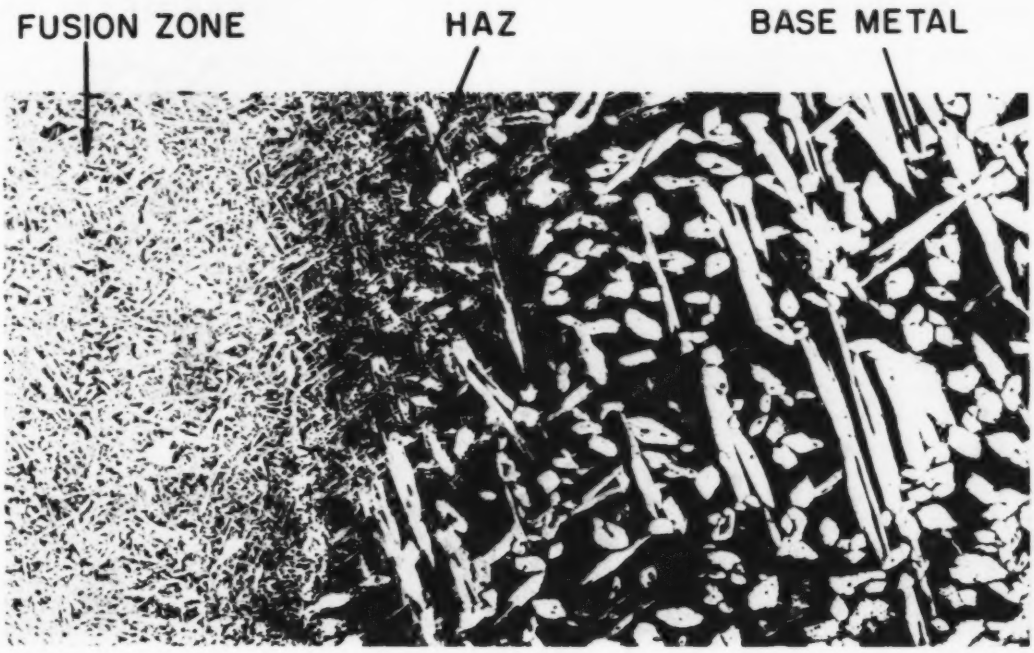

(c) weld 2072-2, 9.7% Al, Ampcotrode 46 filler wire. (neg 3291)

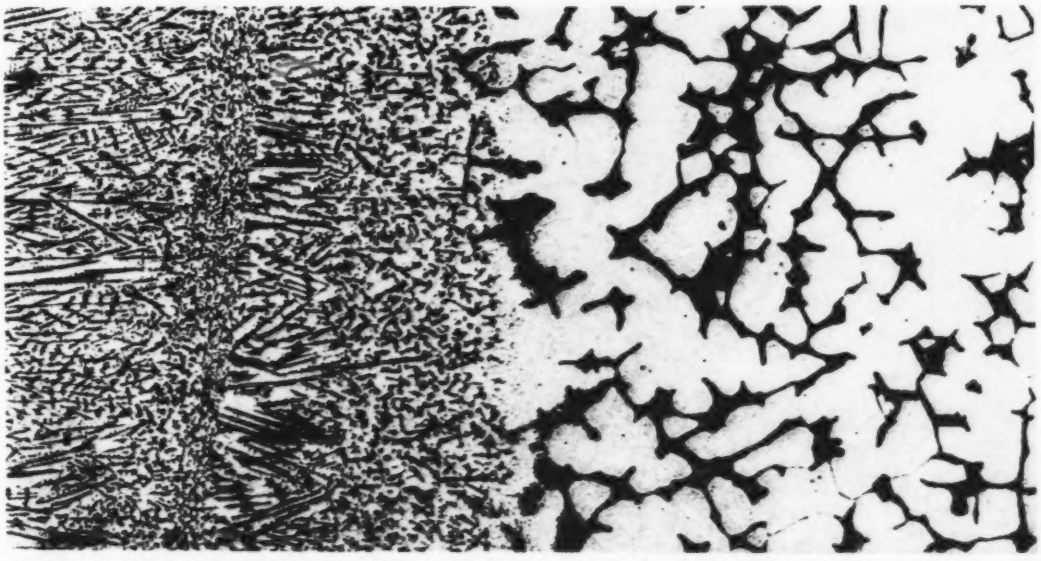

(d) weld 2236-1, 8.58% Al, New low aluminum filler wire. (neg 5867)

Fig. 28. Optical micrographs of weldments at various aluminum contents and for different filler wires. Alcoholic ferric chloride etch. X100.

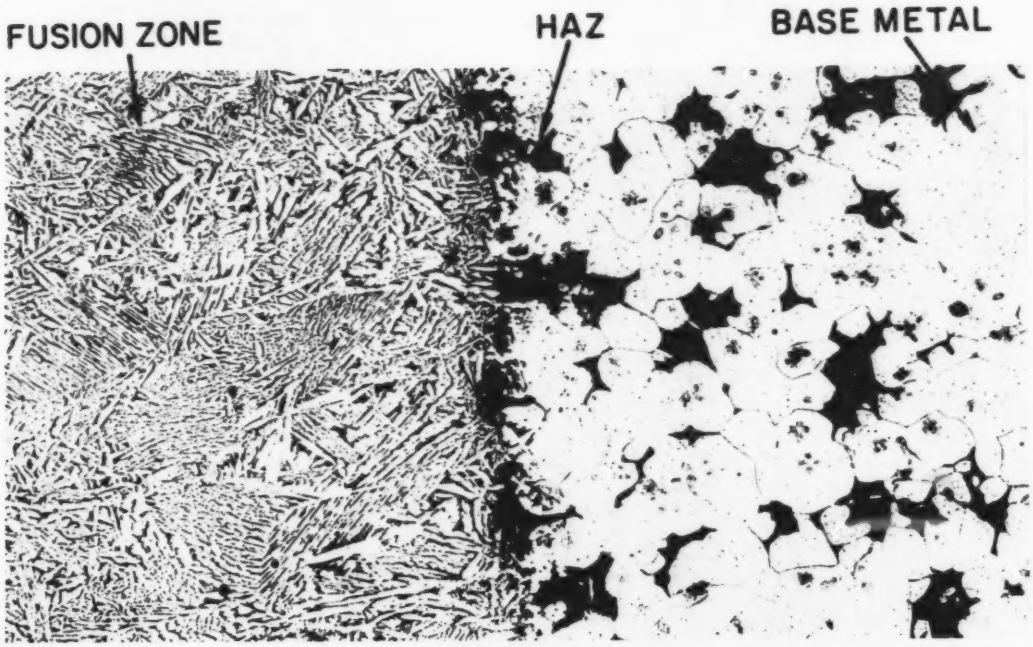

(e) weld 2050-2, 8.35% Al, Ampcotrode 10 filler wire. (neg 5868)

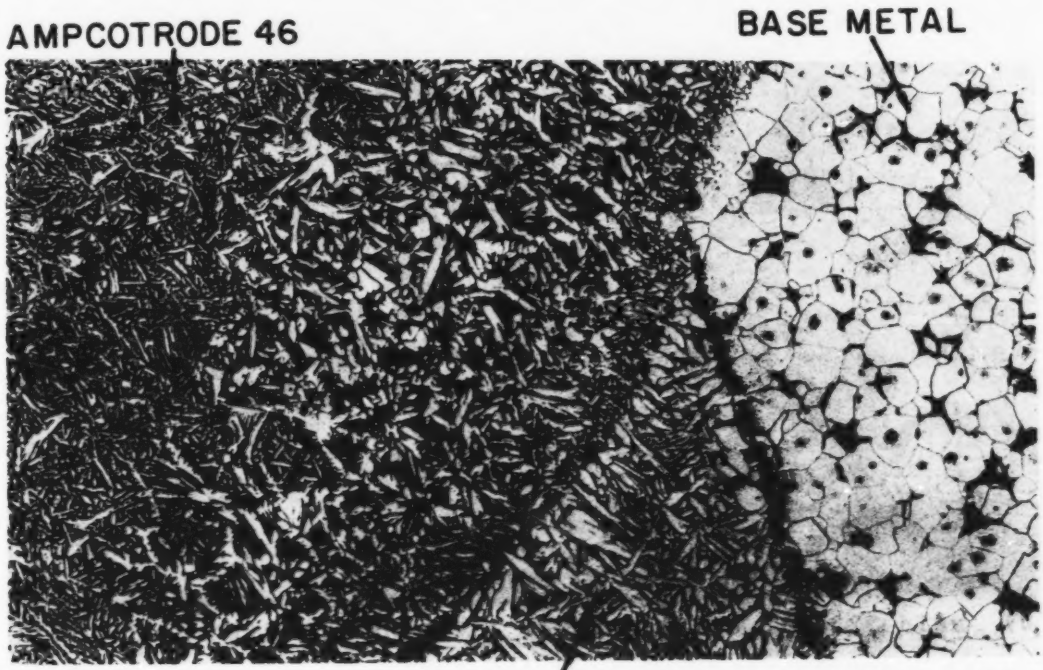

(f) weld 2149-1, 8.28% Al, Ampcotrode 10 and 46 filler wires. (neg 5

Fig. 28. Optical micrographs of weldments at various aluminum contents and fo r different filler wires. Alcoholic ferric chloride etch. X100.

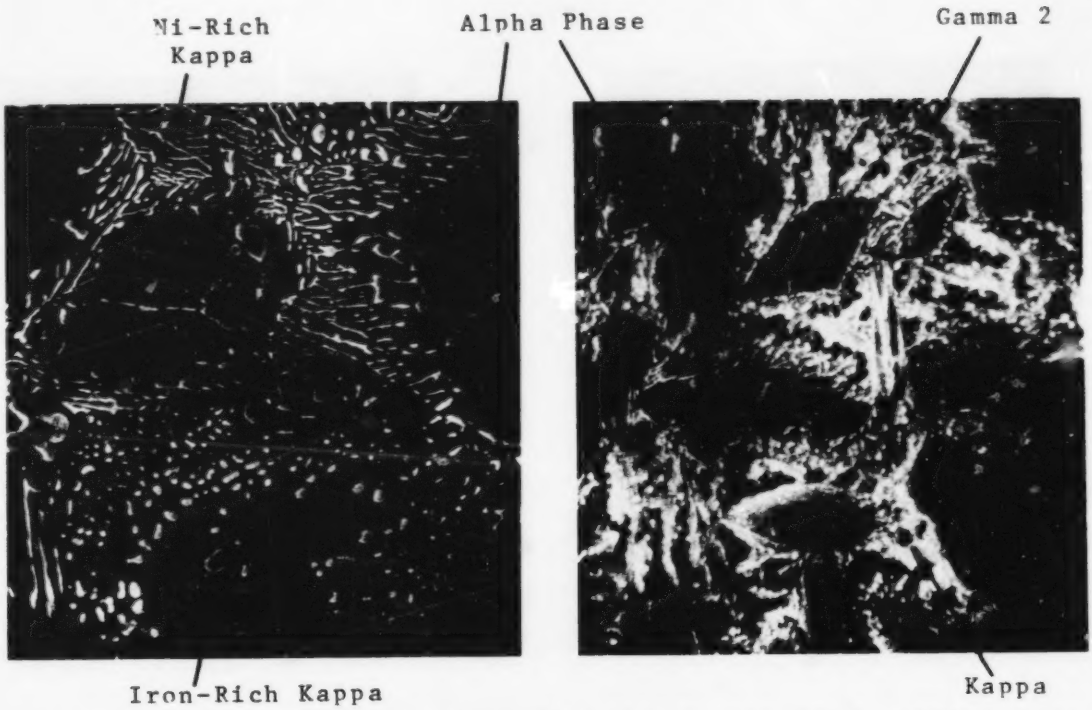

(a) Base metal, X2400. (neg 3278) (b) Fusion zone, X5500. (neg 3279)

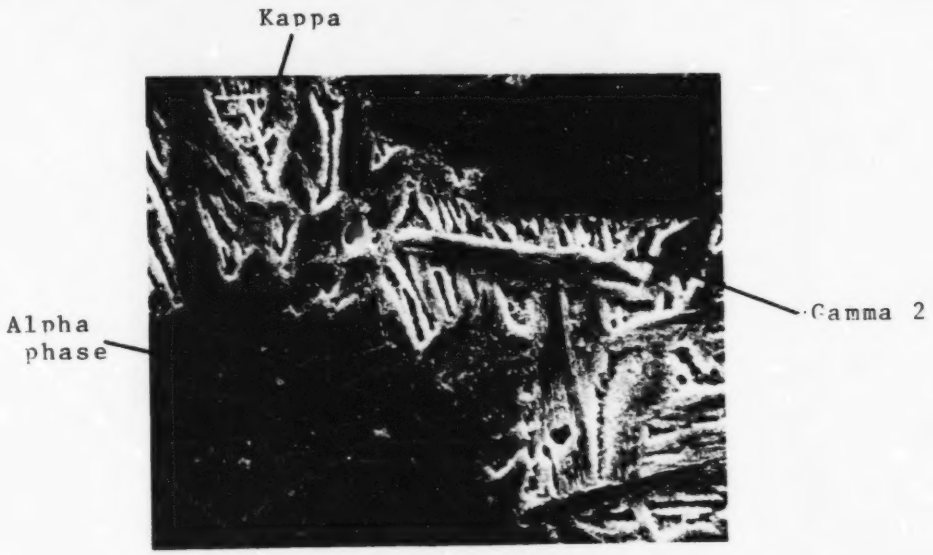

(c) HAZ, X2300. (neg 3276)

Fig. 29. Scanning electron micrographs of weldment 2057-2 (9.1% Al, 4.5% Ni, 4.53% Fe and 1.07% Mn) showing the secondary phases in the as-welded condition. Ampcotrode 46 filler wire. Alcoholic ferric chloride etch.

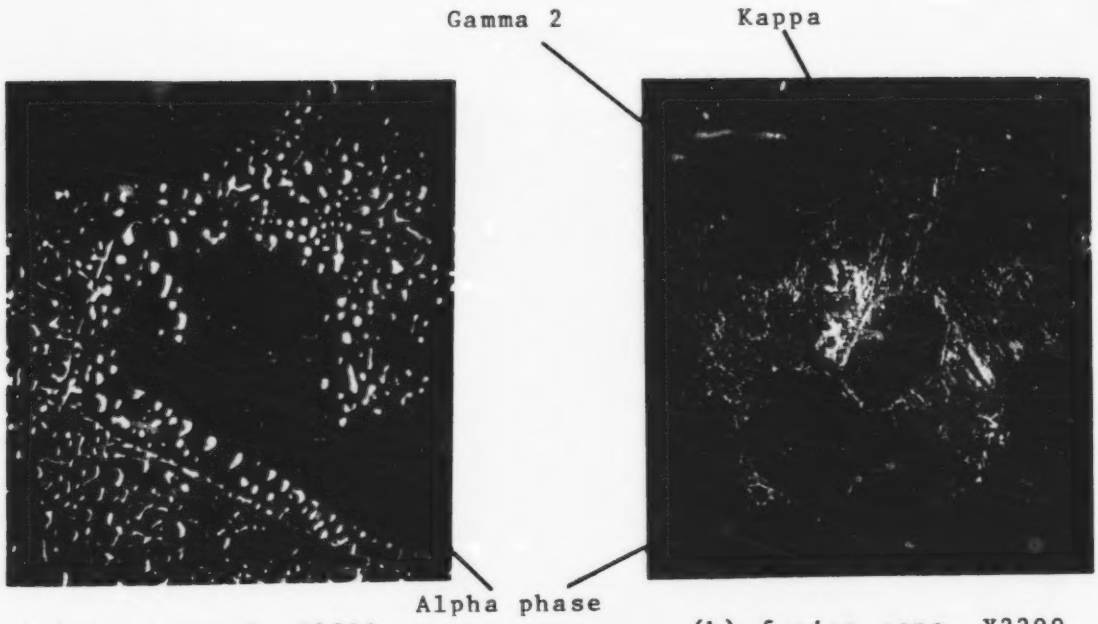

(a) base metal, X2300 (neg 5858)

(b) fusion zone, X2200 (neg 5862)

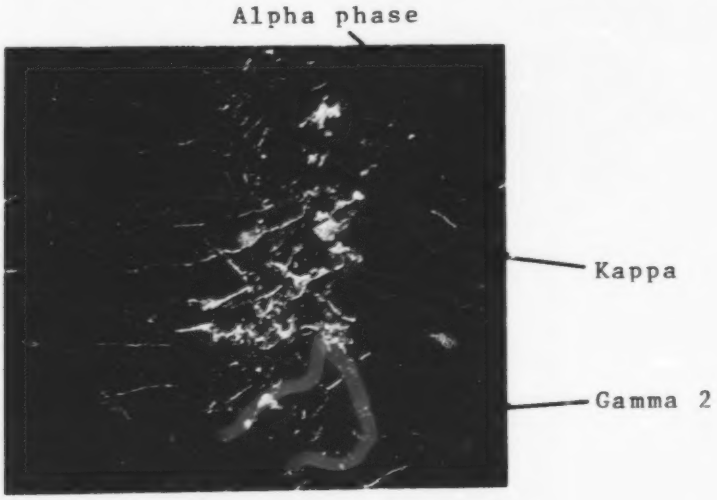

(c) HAZ, X22000 (neg 5859)

(c) HAZ, X2200

Fig. 30. Scanning electron micrographs of weldment 2236-1 (8.58% Al, 4.57% Ni, 3.79% Fe and 0.97% Mn) showing the secondary phases in the as-welded condition. New low aluminum filler wire. Alcoholic ferric chloride etch.

(a) base metal, X2000. (neg 3273)

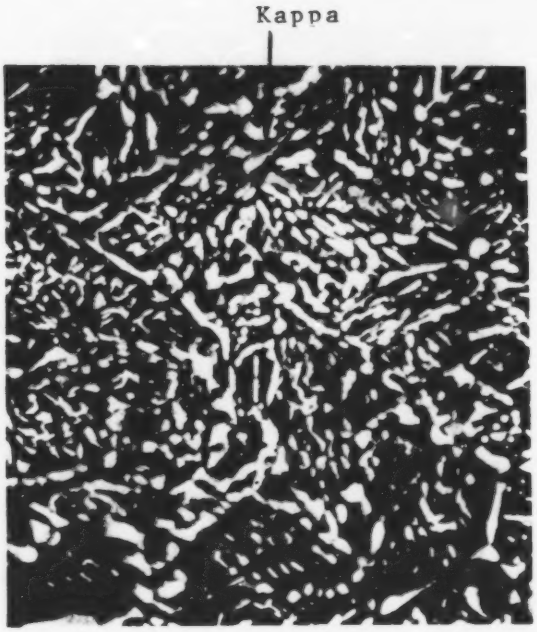

(b) fusion zone, X4600. (neg 3275)

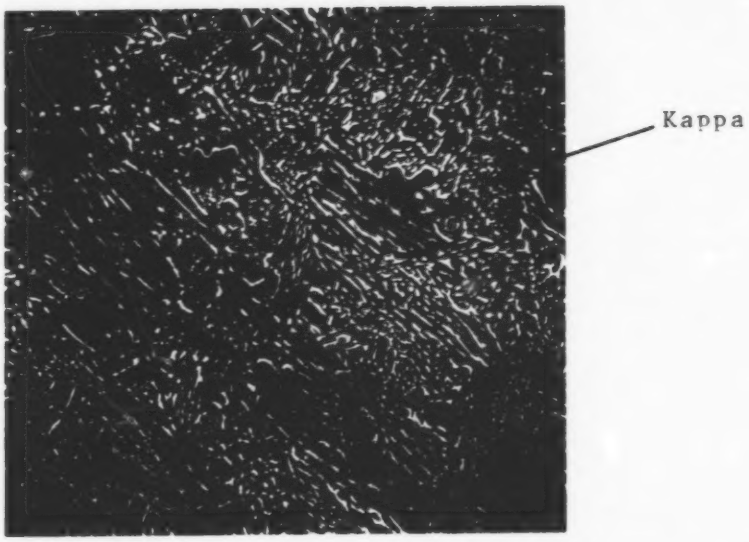

(c) HAZ, X2000. (neg 3274)

Fig. 31. Scanning electron micrographs of weldment 2057-2 (9.1% Al, 4.5% Ni, 4.53% Fe and 1.07% Mn) showing the phases in the post-weld heat treated (700C, 6h) condition. Ampcotrode 46 filler wire. Alcoholic ferric chloride etch.

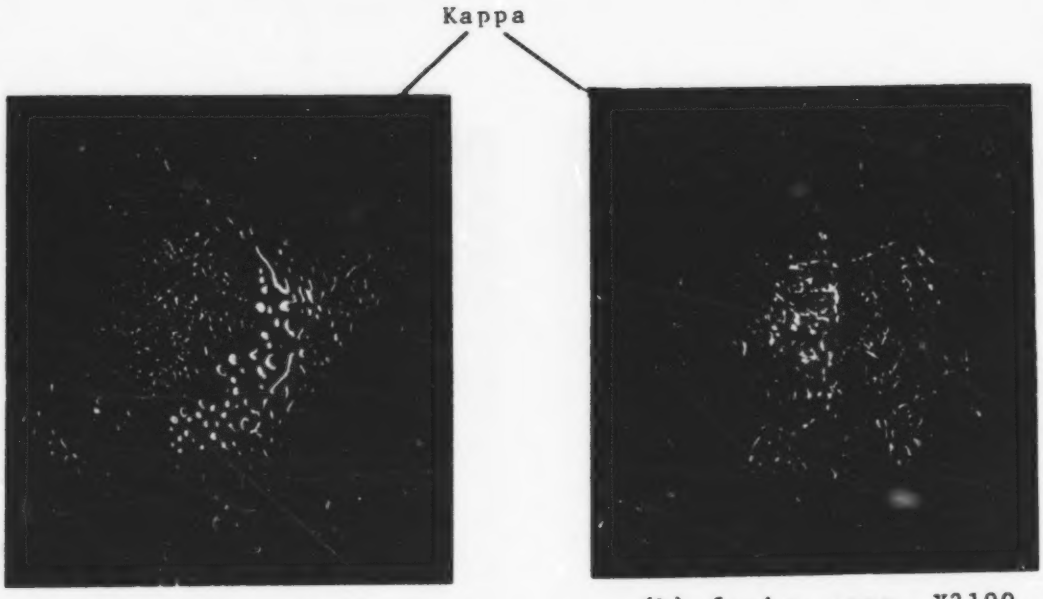

(a) base metal, X2100. (neg 5861)

(b) fusion zone, X2100. (neg 5863)

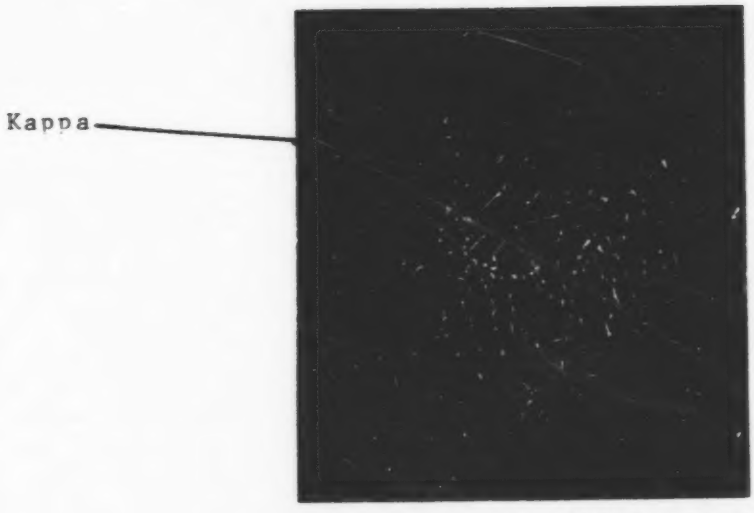

(c) HAZ, X2100. (neg 5860)

Fig. 32. Scanning electron micrographs of weldment 2236-1, (8.58% Al, 4.57% Ni, 3.79% Fe and 0.97% Mn) showing the phases in the post-weld heat treated (700C, 6h) condition. New low aluminum filler wire. Alcoholic ferric chloride etch.

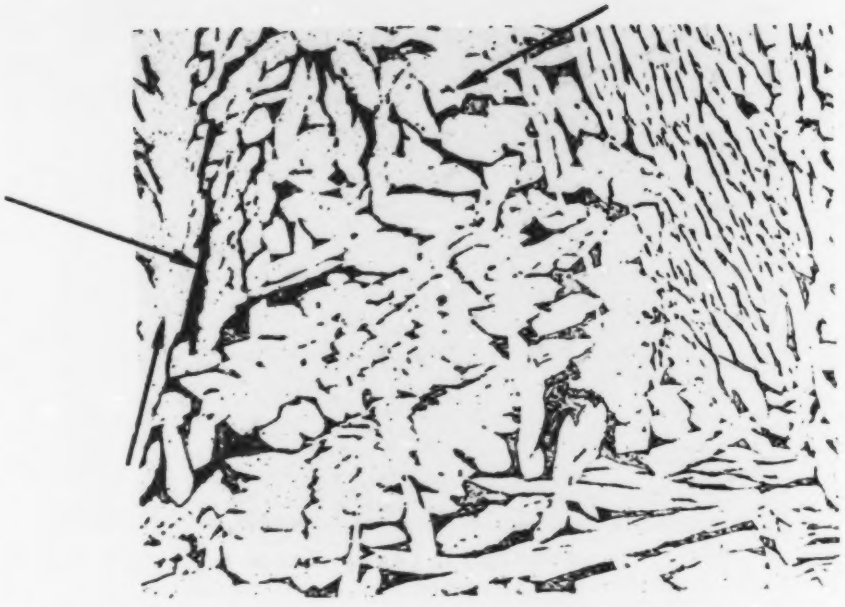

(a) as-welded, optical. X500 (neg 5901)

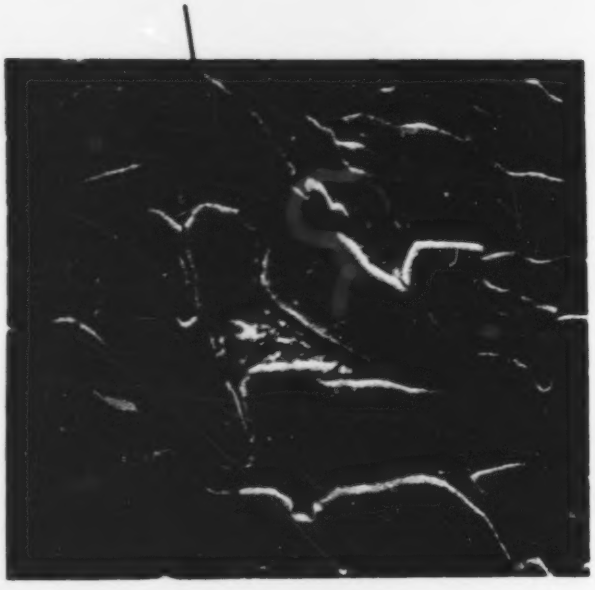

(b) as-welded, SEM. X2300. (neg 5073)

Fig. 33. Optical and scanning electron micrographs of weld 2150-2 (8.35% Al, 4.58% Ni, 5.24% Fe and 1.08% Mn) showing the microstructure of the fusion zone for the as-welded and post-weld heat treated (700C, 6 h) conditions. Ampcotrode 10 filler wire. Alcoholic ferric chloride etch.

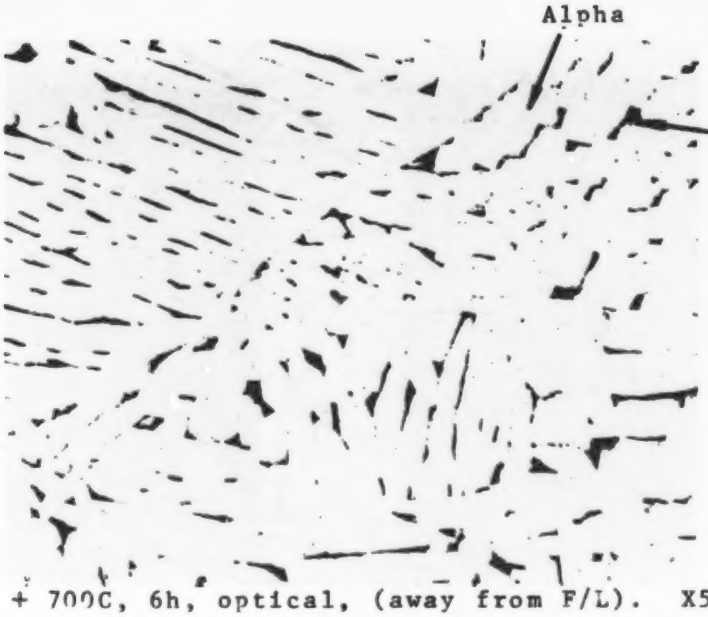

(c) welded + 700C, 6h, optical, (away from F/L). X500

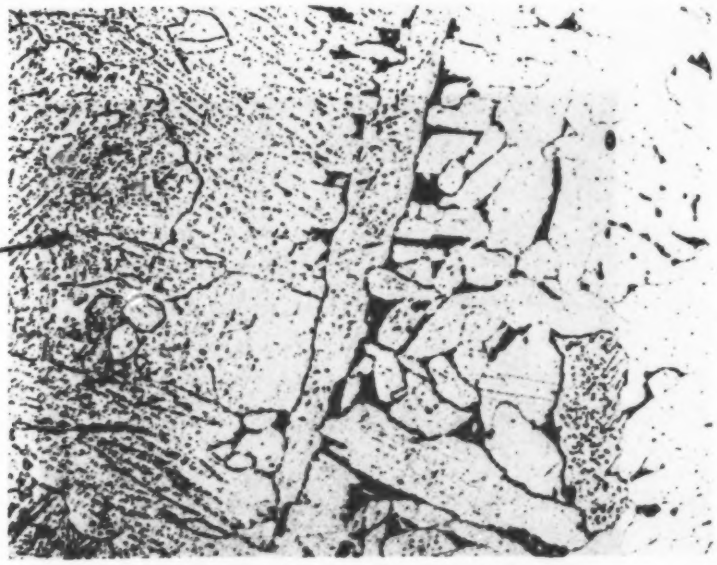

(d) welded + 700C, 6h, optical,(Partially decomposed, close to F/L). X500.

Fig. 33. Optical and scanning electron micrographs of weld 2150-2 (8.35% Al, 4.58% Ni, 5.24% Fe and 1.08% Mn) showing the microstructure of the fusion zone for the as-welded and post-weld heat treated (700C, 6h) condition. Ampcotrode 10 filler wire. Alcoholic ferric chloride etch.

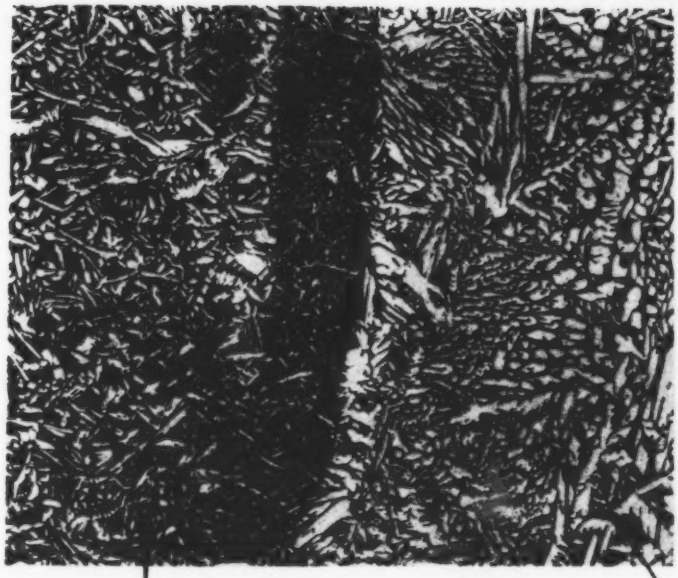

(neg 5870)

(a) as-welded, X100.

Ampcotrode 46

Ampcotrode 10

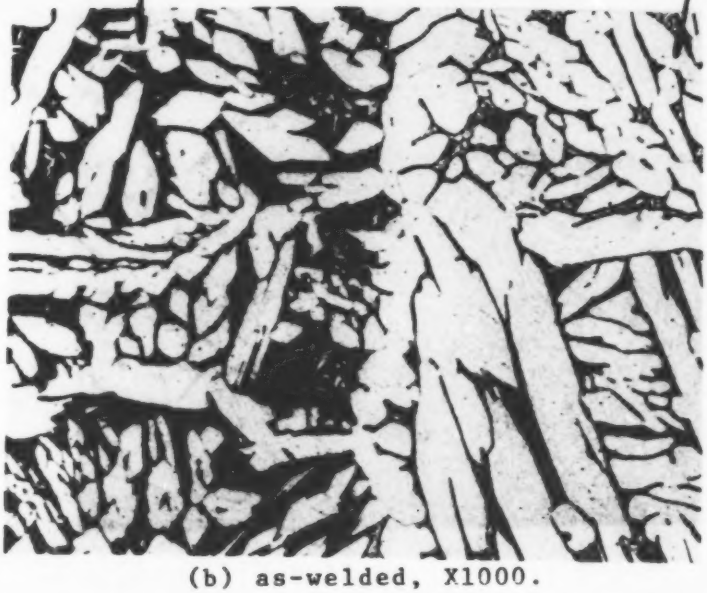

(neg 5898)

(b) as-welded, X1000.

Fig. 34. Optical micrographs of the fusion zone of weld 2148-1 (8.25% Al, 4.88% Ni, 5.08% Fe, and 1.05% Mn) showing the transition between filler wires Ampcotrode 10 and 46. Alcoholic ferric chloride etch.

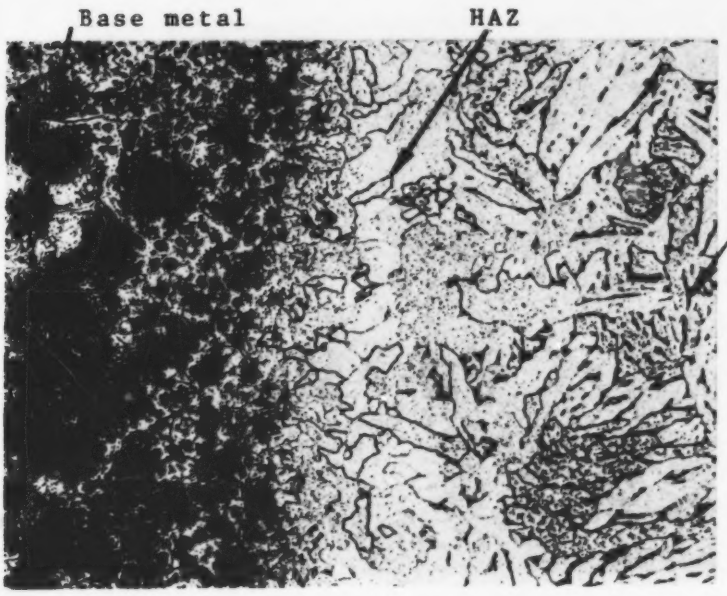

(c) welded + 700C, 6h, X200. (neg 5872)

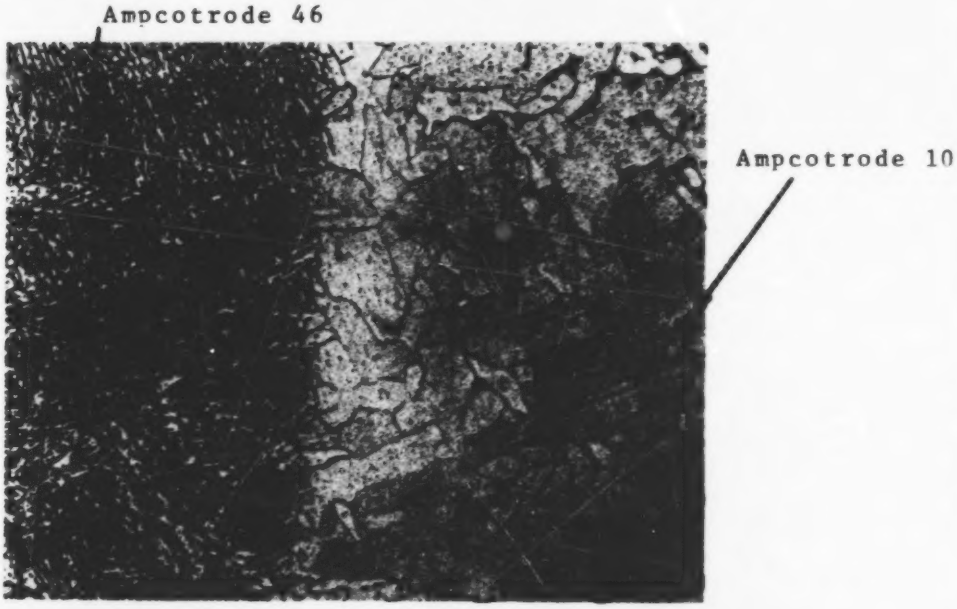

(d) welded + 700C, 6h, X500. (neg 5902)

Fig. 34. Optical micrographs of the fusion zone of weld 2148-1 (8.28% Al, 4.88% Ni, 5.08% Fe and 1.05% Mn) showing the transition between filler wires Ampcotrode 10 and 46. Alcoholic ferric chloride etch.

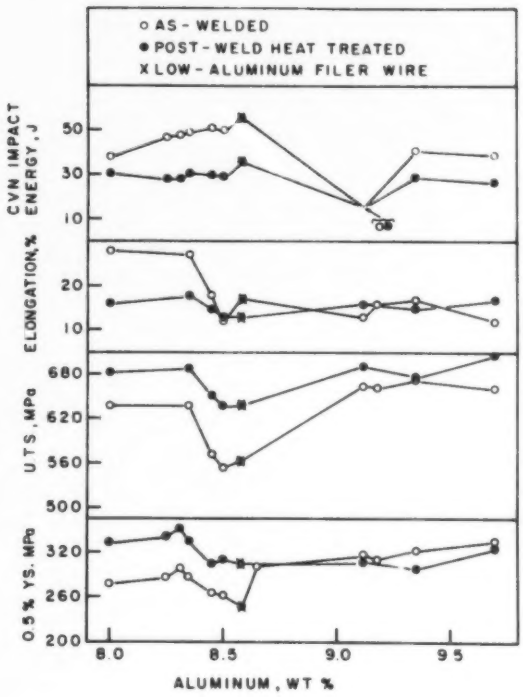

Fig. 35. Mechanical properties of NAB alloys in the as-welded and post-weld heat treated condition. (Specimens cut from welded plates - weld at centre of gauge length). (neg 6043)